Pergamon

PII: S0967-0637(96)00059-3

Deep-Sea Research I, Vol. 43, No. 8, pp. 1273–1304, 1996

0967-0637/96 $15.00 + 0.00

Measured and modeled primary production in the northeast Atlantic (EUMELI JGOFS program): the impact of natural variations in photosynthetic parameters on model predictive skill

ANDRÉ MOREL,* DAVID ANTOINE,* MARCEL BABIN* and YVES DANDONNEAU†

(*Received* 20 *June* 1995; *in revised form* 14 *February* 1996; *accepted* 27 *April* 1996)

Abstract—Use of ocean color satellite data in global biogeochemical studies requires models to predict primary production from the satellite-derived chlorophyll fields. In this paper, measured bio-optical and photo-physiological data are used in place of standard (constant) parameters to adjust a previously published primary production model. In the JGOFS–France program, systematic studies were carried out at three locations in the tropical northeast Atlantic, selected to represent typical EUtrophic, MEsotrophic and oLIgotrophic regimes (EUMELI cruises). During cruise no. 4, these studies included the spectral measurements of the photosynthetically available radiation at sea level and within the water column, the determination of the algal absorption spectra and the determination of the physiological parameters derivable from P versus E experiments (photosynthesis–irradiance responses). The model predictions are compared with *in situ* determinations made by the ^{14}C technique (JGOFS core parameter).

At the three sites, the physical structure (mixed layer and euphotic depths), the algal abundance and community structure, as well as their bio-optical and physiological properties, are very different, so that the predictive performance of the model was tested in trophic conditions that span most of those expected in the global open ocean. The model, when adjusted by entering the actual physiological parameters (chlorophyll-specific absorption of algae, maximum quantum yield, and light saturated carbon fixation rate), provides satisfying results compared to those observed *in situ*. The relative roles of the physiological parameters are analyzed and sensitivity studies are performed.

For global applications, and in the absence of specific information when all seasons and provinces of the world ocean are considered, it will remain necessary for a while to rely on generic models and a selected standard set of physiological properties. The sensitivity studies here presented help in this choice, and a modified set of parameters is proposed and tested. With this set, reconstructed production profiles are close to those determined in the field, and the integrated values are retrieved with no bias and a reduced scatter (18% at one SD) for 17 stations (cruises 3 and 4) and daily production ranging from 0.3 to 2.3 gC m^{-2}. Copyright © 1996 Elsevier Science Ltd

INTRODUCTION

One of the major objectives of the Joint Global Ocean Flux Study (JGOFS) was specifically to "use satellite data of ocean color and other remotely-sensed data to provide a global, time-varying, picture of phytoplankton and primary production". This objective requires that in "various representative ocean regimes" process studies be carried out to "assess the

* Laboratoire de Physique et Chimie Marines, Université Pierre et Marie Curie and CNRS, BP 8, F-06230, Villefranche-sur-Mer, France.

† LODYC Laboratoire d'Océanographie Dynamique et de Climatologie, Université Pierre et Marie Curie, CNRS, and ORSTOM, 4, place Jussieu, F-5252, Paris Cédex 05, France.

rates of, and controls on, vertically distributed primary production and the degree to which they can be determined using remotely-sensed near-surface pigment data" (JGOFS/SCOR, 1990).

In all studies devoted to biogeochemical cycles and fluxes, from surface layers down to the sea floor, the essential link in the chain is the biological process of primary production by planktonic algae. This process should be considered first and has two consequences, namely the fixation of inorganic dissolved carbon, and the synthesis in the upper lit layers of particulate organic carbon, a portion of which is exported to deeper levels. Therefore, using satellite information for biogeochemical studies at the global scale requires two initial considerations (see e.g. Lewis, 1992): (i) phytoplankton (as detectable from space through the change in ocean color) can be reliably quantified in terms of sea-surface chlorophyll concentration within the upper layer (actually within a factor 2; Gordon and Morel, 1983) and then can be extended downward to encompass the whole productive algal stock (Morel and Berthon, 1989); and (ii) a model is available with the capacity of transforming the chlorophyll fields into primary production "maps" under prescribed temperature and surface irradiance conditions. The accuracy in the pigment retrieval is not discussed here, and the present paper deals only with the second aspect of the problem. It makes use of a spectral light–photosynthesis model previously developed (Morel, 1991) and then validated (Berthon and Morel, 1992). The validation was made by comparing *in situ* determinations of primary production (1987 samples at 337 stations) to model predictions based on chlorophyll concentration as input. This validation exercise, based on historical data, showed that, over more than 3 orders of magnitude in chlorophyll concentration, the skill in prediction of primary production was acceptable. Computed and measured productions agreed within a factor of about 3 over 2.5 orders of magnitude in terms of daily column-integrated production. Improvements, however, are definitely desirable. More accurate predictions can be reached through a better understanding of the algal photo-physiological characteristics introduced into the computations.

In line with the JGOFS recommendations, a French JGOFS program, under the acronym EUMELI, was created. It consisted of systematic biogeochemical studies at three sites, which were selected with a view to representing typical EUtrophic, MEsotrophic and oLIgotrophic regimes. These sites are located in the tropical eastern Atlantic Ocean approximately along the 20°N parallel (see map, Fig. 1). Therefore, similar climatic conditions (solar irradiation, surface heat flux) characterize the three locations, while the concentration and community structure of the algal standing stocks are very different. Along the Mauritanian coast and in response to persistent trade winds, nutrient-rich upwelled waters support dense phytoplankton populations. A previous study (Bricaud *et al.*, 1987), based on CZCS (Coastal Zone Color Scanner) data, demonstrated that, in spite of seasonal fluctuations, chlorophyll-rich waters are always present in the vicinity of Cape Blanc, as a result of favorable conditions for a permanent upwelling (Speth and Detlefsen, 1982). Therefore, the EUMELI eutrophic site was selected in this upwelling area, and the sampling station, positioned about 140 km off this cape, is outside of the turbid waters that remain confined within a rather narrow band along the Mauritanian coast (Morel, 1982; Bricaud *et al.*, 1987). The selected oligotrophic site was located about 1400 km offshore and thus at the periphery of the stable North Atlantic gyre, where oligotrophic conditions persist year-round. This regime was confirmed by an examination of the CZCS archive (Feldman *et al.*, 1989), showing chlorophyll concentration around 0.07 mg m^{-3} (see Fig. 2). The choice of a site representative of intermediate trophic conditions was more difficult and somewhat

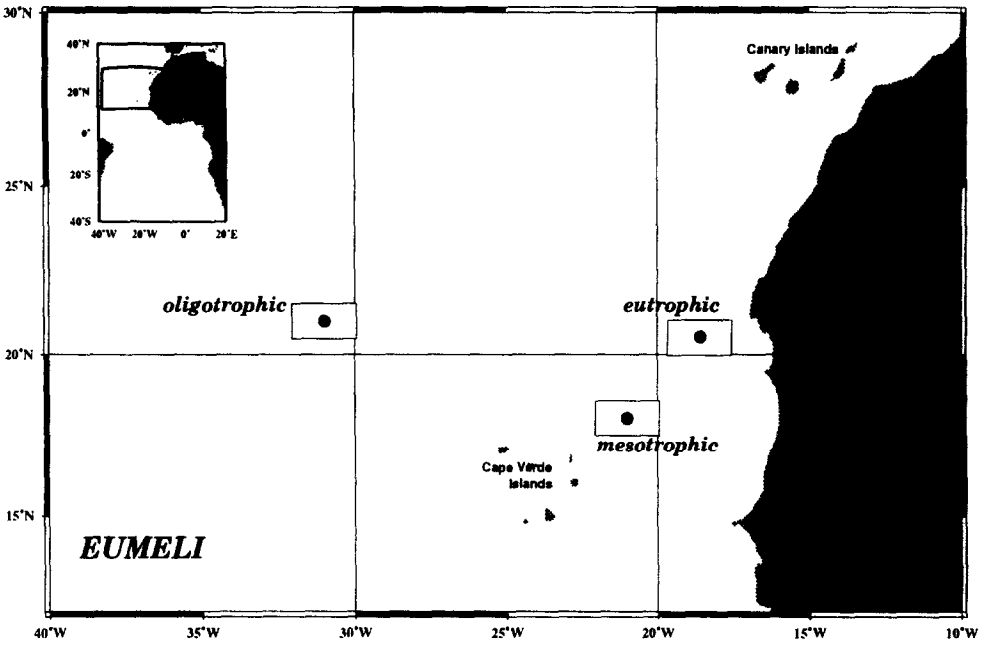

Fig. 1. Location of the three sites selected for the EUMELI program. The rectangles show the pixel-grouping used in Fig. 2.

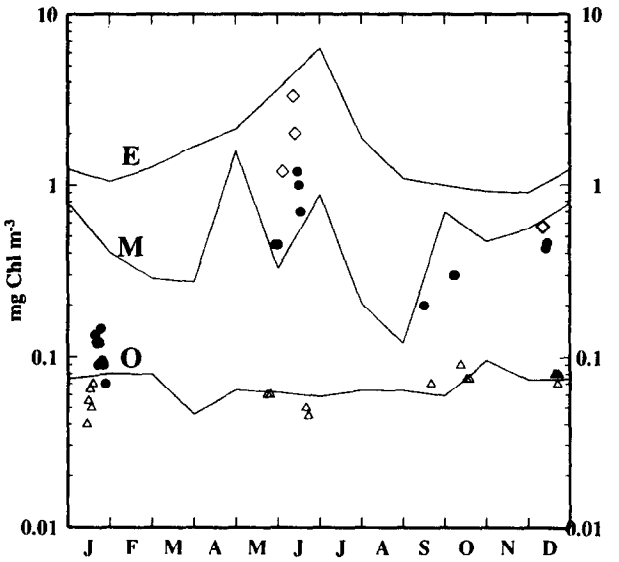

Fig. 2. Annual cycle of the chlorophyll concentration at the three EUMELI sites. These values are extracted from 12 "climatological monthly mean" global chlorophyll images derived from the CZCS archive (Feldman *et al.*, 1989) and are computed by averaging over a 117 × 218 km rectangle centered on each site. Upper layer chlorophyll concentrations at the three sites, measured during several EUMELI cruises, namely no. 2 (January), no. 3 (September–October), no. 4 (May–June) and no. 5 (December) are also shown with the following symbols: diamonds, closed circles, and triangles for eutrophic, mesotrophic, and oligotrophic sites, respectively..

debatable, to the extent that mesotrophic regimes in this zone seem to be transient rather than permanent. While drifting offshore from the coastal upwelling sources, surface waters often create extended filaments reaching the Cape Verde islands, with distinct chlorophyll signatures (Bricaud *et al.*, 1987). Such features vary in time and space according to the intensity of horizontal advection and wind stress. Therefore the selected mesotrophic site, located about 400 km offshore, was admittedly in unsteady equilibrium, and was expected to oscillate between quasi-eutrophic and nearly oligotrophic regimes. On average however, and despite oscillations, its mesotrophic character is clearly demonstrated by the mean annual value of the chlorophyll concentration centered on 0.5 mg m^{-3} on average (Fig. 2).

In the Morel (1991) primary production model (as in some others, e.g. Platt *et al.*, 1988; Platt and Sathyendranath, 1988; Sathyendranath *et al.*, 1989; Smith *et al.*, 1989; Wozniak *et al.*, 1992), optical phenomena are accurately described, and the functional dependency of photosynthesis on radiative energy is mathematically expressed in a precise manner. The weakness lies in the numerical values assigned to several physiological parameters used as inputs in these mathematical expressions.

When the model is operated at large scale, "standard" mean values of physiological parameters are used because of lack of sufficient and specific information. These parameters, which quantify photo-physiological characteristics of algae, such as radiation capture capacity, quantum yield of the net photosynthesis, maximum photosynthetic rate, photoinhibition, etc., are modulated by environmental forcing. They are known to vary with location, depth and time at various frequencies, from diel to seasonal timescales (see e.g. Cullen *et al.*, 1992a). Changes in species composition represent a parallel consequence of environmental forcing. Several attempts have been made to predict variations of photo-physiological characteristics by accounting for the kinetics of algal photoacclimation in turbulent systems (Lewis *et al.*, 1988; Cullen and Lewis, 1988; Lande and Lewis, 1989). Nevertheless, although trends were clearly identified, a comprehensive knowledge of all kinds of physiological responses and their very causes is far from being sufficiently documented and quantified. Therefore, local parameters are not reliably predictable, so that variations cannot presently be introduced in any model when global applications are envisaged. For example, in previous applications to CZCS data of the model of Morel (1991), at regional (Morel and André, 1991; Antoine *et al.*, 1995) or global scales (Antoine *et al.*, 1996), "standard" mean values were assigned by necessity to physiological parameters, including, however, a simple dependency of the maximum photosynthetic rate upon temperature. A selection of characteristic seasonal values of these parameters for various oceanic domains is made in the studies by Platt *et al.* (1991), Sathyendranath *et al.* (1995) and by Longhurst *et al.* (1995), which aim at computing global primary production. To assess the consequences of such choices or simplifying approximations, one goal of the EUMELI program was to determine the range of variation of these parameters in markedly differing, supposedly representative, oceanic regimes.

A series of questions were addressed in this study: (i) Are the results of the light-photosynthesis model, when operated with the standard set of physiological parameters, acceptable, fair, or erroneous if compared with specific field data, and, in the last case, for what reasons? (ii) What are the achievable improvements when the model is "adjusted", i.e. operated with locally pertinent values given to the photo-physiological parameters? (iii) What are the more influential parameter adjustments for successful computation? (iv) Knowing their respective influences on the predictive skill of the model, is it possible to make improvements by adopting a more realistic set of parameters?

To address such questions it is necessary to determine, for various depths, the physiological parameters derivable from P versus E experiments (photosynthesis–irradiance curves). Namely the maximum quantum yield for growth, $\varphi_{\mu max}$, the irradiance level that determines the onset of the light-saturated photosynthesis regime, denoted E_k (Talling, 1957; see also the Appendix) and the level of production in this regime, $P^B{}_{max}$, are required. It is also necessary to know the light harvesting capacity of local phytoplankton, i.e. their spectral Chl-specific absorption coefficients, denoted $a^*(\lambda)$. Other data are also needed, namely the temperature profile and the photosynthetically available radiation (PAR) incident at sea level or within the water body. Then by using as input the measured Chl(z) profiles, the outputs of the model, operated in its standard or adjusted mode, can be compared to "sea-truth" measurements, consisting of *in situ* primary production, measured at various levels within the entire productive column.

During leg 2 of EUMELI cruise no. 4 (June 1992), all the above determinations were systematically performed at the three sites. With this data set, the questions listed above are examined in the present paper. During the first leg of this cruise, only the *in situ* primary production experiments (and chlorophyll determinations) were carried out; these additional results, as well as those obtained eight months earlier (EUMELI, cruise no. 3, for the meso- and oligotrophic sites) are used as a test data set for the adjusted and standard models.

MATERIALS AND METHODS

In vitro *measurements*

According to a technique described by Bricaud and Stramski (1990), the absorption spectra of particulate matter collected onto a wet GF/F filter were determined by using a LI-COR spectroradiometer (LI-1800 UW) equipped with an integrating sphere. The pathlength amplification (or β factor, Butler, 1962), inherent to the filter technique, was estimated by using the relationship proposed by Bricaud and Stramski (1990), and the absorption values were corrected accordingly. The extractive bleaching method developed by Kishino *et al.* (1985, 1986) was used to determine the absorption spectrum of non-pigmented (and depigmented) particles. By subtracting this non-living material absorption from the total absorption, the absorption coefficients for the algae alone were derived, and then divided by the amount of chlorophyll (actually the sum of Chl *a* and divinyl-Chl *a* as determined by HPLC) to derive the chlorophyll-specific coefficients, $a^*(\lambda)$. When the extractive method was not applied, the numerical method described in Bricaud and Stramski (1990) was used to compute the algal absorption coefficients. Examples of the $a^*(\lambda)$ spectra determined at the three sites are presented in Babin *et al.* (1996).

The photosynthesis–irradiance (P versus E) curves were determined with a 10 chamber incubator, equipped with a 250 W lamp of known spectral exitance and neutral filters. With 12 irradiance levels in each chamber, the photosynthetic response curve for each sample was determined (Babin *et al.*, 1994) and then fitted by a hyperbolic tangent function (Jassby and Platt, 1976). From these curves, the initial slope, α, the maximum photosynthetic rate, P_{max}, and therefrom the saturation onset irradiance, E_k ($=P_{max}/\alpha$), were computed. The maximum quantum yield for growth, $\varphi_{\mu max}$, was derived from α, knowing the phytoplankton absorption spectrum and the incubator lamp irradiance spectrum (details in the Appendix). In each experiment, 10 samples originating from 10 depths were

simultaneously analyzed; about 200 P versus E curves were determined during leg 2, and some examples from the three sites are displayed in Fig. 3.

On the same samples used for the absorption and P versus E, the pigment composition was analyzed by HPLC (Claustre and Marty, 1995). On a few occasions, the HPLC determination was replaced by spectrofluorometric determination, with the appropriate conversion factor to ensure internal consistency (see Babin *et al.*, 1996). As for absorption, after dividing by the sum of Chl *a* and divinyl-Chl *a* content, the photosynthesis parameters were transformed into Chl-specific quantities, denoted α^B and P^B_{max}, and expressed as $g\,C\,(g\,Chl)^{-1}\,(mol\,quanta\,m^{-2})^{-1}$ and $g\,C\,(g\,Chl)^{-1}\,h^{-1}$, respectively (see also the Appendix and Tables 1 and 2).

Because each site was occupied for several days (Table 3), phytoplankton optical properties and photosynthetic parameters were determined with depth over a number of days and several times a day. In the calculations described below, vertical profiles of these properties, averaged for each site, are used (Figs 6–8 of this paper; the variability can be seen in Babin *et al.*, 1996).

In situ *measurements*

Regular (every 3 h) hydrographic casts were performed (CTD, SeaBird SBE 11 Plus mounted onto a rosette), providing temperature, salinity and density profiles, as well as Chl-fluorescence and beam attenuation coefficient profiles (Sea Tech sensors). Nutrient determinations at the micro- and nano-molar levels were made on a regular basis according to a method described by Raimbault *et al.* (1990).

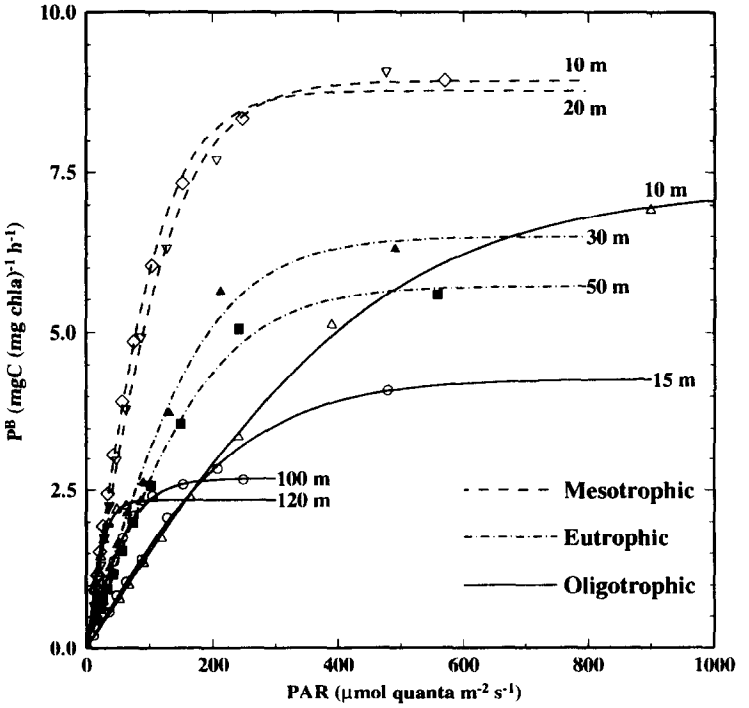

Fig. 3. Examples of P–E curves determined at the three sites and at various depths, as indicated.

Table 1. *Constant photo-physiological parameters used in the standard model (versions* 1 *and* 2, *see text)*

	a^*_{max}	$\varphi_{\mu max}$	α'^B	KPUR	P^B_{max}
Version 1	45	0.07	37.8	25.1	3.41
Version 2			16	80.0	4.61

Units are: a^*_{max} in m^2 (g Chl)$^{-1}$, $\varphi_{\mu max}$ in mol C (mol quanta)$^{-1}$, α'^B in g C (g Chl)$^{-1}$ (mol quanta m^{-2})$^{-1}$ (see equation (2b)); KPUR in μmol quanta m^{-2} s^{-1} (value at 20°C); and P^B_{max} in g C (g Chl)$^{-1}$ h^{-1} (computed via (A8), see the Appendix).

Primary production was measured *in situ* with the "let go" device developed by Dandonneau and Le Bouteiller (1992) and in conformity with the JGOFS recommendations (clean techniques and 24 h incubation). The let go device automatically isolates and immobilizes the sample at depth within a transparent sphere, and simultaneously injects the ^{14}C. This technique avoids possible artifacts that may arise when flasks are handled on board. The carbon fixation measured by this device, however, cannot be related to the chlorophyll concentration within the specific sample. It is necessary to rely on the pigment determination made on samples from the same depth taken during the CTD casts immediately before and after the deployment of the let go. This procedure may cause some discrepancies when the biomass distribution is spatially and temporally heterogeneous.

During leg 2, cruise no. 4, the spectral composition of irradiance (downwelling and upwelling) at various depths and the spectrally integrated irradiance (PAR) profiles were measured daily as previously described (e.g. Morel, 1988). Typical examples of the contrasting optical properties of the waters at the three sites are displayed in Fig. 4. In Case 1 waters with high chlorophyll concentration occuring at the eutrophic site, green light (centered on 560 nm) dominated, while blue light (centered on 480 nm) characterized the oligotrophic site. An intermediate situation was observed at the mesotrophic site, with a

Table 2. *Mean values of the photo-physiological parameters determined at the three sites; three layers are identified at the oligotrophic site. They are given merely for comparison with the standard parameters in Table* 1, *as the adjusted model makes use of the depth-dependent values (Figs* 6, 7, *and* 8, *panels a and b). The last two columns provide the* P^B_{max} *values, computed from the standard values of Table* 1 *using the actual temperatures at each site and layer. Same symbols and units as in Table* 1

Site	a^*_{max}	$\varphi_{\mu max}$	α'^B	KPUR	P^B_{max}	P^B_{max}	
						Version 1	Version 2
Eutrophic	32	0.05	21.1	60	5.5	2.97	4.02
Mesotrophic	100	0.025	30	100→60*	10→6	3.70	5.00
Oligotrophic:							
Mixed layer	165	0.006	12	230→70	7→4	4.48	6.06
DCM layer	150→110	0.01→0.04	18→48	35→20	4→2.5	3.89	5.26
Below DCM	80	0.06	57	20→10	2	3.63	4.90

†When two values are given, they indicate the vertical trend within the layer in question.

Table 3. Daily column integrated primary production (g C m^{-2}); *the relative differences with respect to measured* in situ *values are given in parentheses (as %)*

Site and cruise	Leg	Date	Measured	Computed (adjusted model)	Computed (standard model)	
					Version 1	Version 2
Eutrophic						
Cruise 4	2	13 June	2.279	2.666 (+17.0)	2.202 (−3.3)	2.057 (−10.0)
(1992)		14 June	1.749	2.235 (+28.0)	1.884 (+7.7)	1.750 (0.0)
	1	5 June	1.292	1.573 (+21.0)	1.398 (+8.2)	1.289 (0.0)
Mesotrophic						
Cruise 4	2	16 June	1.619	2.819 (1.905)* (+17.7)	1.445 (−10.7)	1.442 (−11.0)
		17 June	1.204	2.464 (1.403)* (+16.5)	1.354 (+12.5)	1.231 (+2.2)
		18 June	(0.946)†	2.237 (1.476)*	1.187	1.144
	1	31 May	0.940	1.615 (+72.0)	0.879 (−6.5)	0.851 (−9.5)
		2 June	0.938	1.580 (+68.0)	0.889 (−5.0)	0.797 (−15.0)
Cruise 3	—	16 September	0.525	1.277 (+143.0)	0.781 (+49.0)	0.592 (+12.7)
(1991)		8 October	0.521	1.994 (+282.0)	1.192 (+128.0)	0.815 (+56.0)
Oligotrophic						
Cruise 4	2	22 June	0.314	0.340 (+8.0)	0.374 (+19.0)	0.298 (−5.0)
		24 June	0.376	0.332 (−12.0)	0.374 (0.0)	0.291 (−22.0)
	1	25 May	0.279	0.368 (+32.0)	0.403 (+44.4)	0.327 (+17.2)
		27 May	0.396	0.357 (−10.0)	0.380 (−6.0)	0.309 (−12.0)
Cruise 3	1	21 September	0.289	0.403 (+39.5)	0.437 (+51.2)	0.297 (+2.8)
	2	13 October	0.313	0.406 (+29.7)	0.529 (+69.0)	0.313 (0.0)
		17 October	0.353	0.353 (0.0)	0.450 (+27.5)	0.265 (−25.0)
		19 October	0.336	0.372 (+10.7)	0.473 (+40.8)	0.279 (−17.0)
Cruise 4 (Eutrophic + Mesotrophic + Oligotrophic)				$N=9$‡	$N=11$	$N=11$
Mean relative error and standard deviation (both as %)				+13.3 (±14.4)	+5.5 (±15.0)	−7.0 (±11.0)
Cruise 3 and 4 (Eutrophic + Mesotrophic + Oligotrophic)					$N=17$	$N=17$
Mean relative error and standard deviation (both as %)					+25.0 (±35.0)	−2.0 (±18.0)

*Computed by using the adjusted model and the measured in-water irradiance values (only for leg 2; no irradiance measurement during leg 1).

†Incomplete profile.

particular feature (dip) originating from the phycoerythrin absorption band due to cyanobacteria and centered on 548 nm. The incident solar irradiance at the surface was permanently monitored on the deck (example in Fig. 5).

Computational aspects

For a given day and latitude, the spectral photosynthesis model (Morel, 1991) predicts the vertical profile of daily primary production from the Chl(z) profile. For the following computations, the model will be forced by the Chl(z) profiles as determined at sea.

Through its atmospheric segment, the model can compute the spectral irradiance at the ocean surface as a function of the solar elevation and for a cloudless sky (see legend of

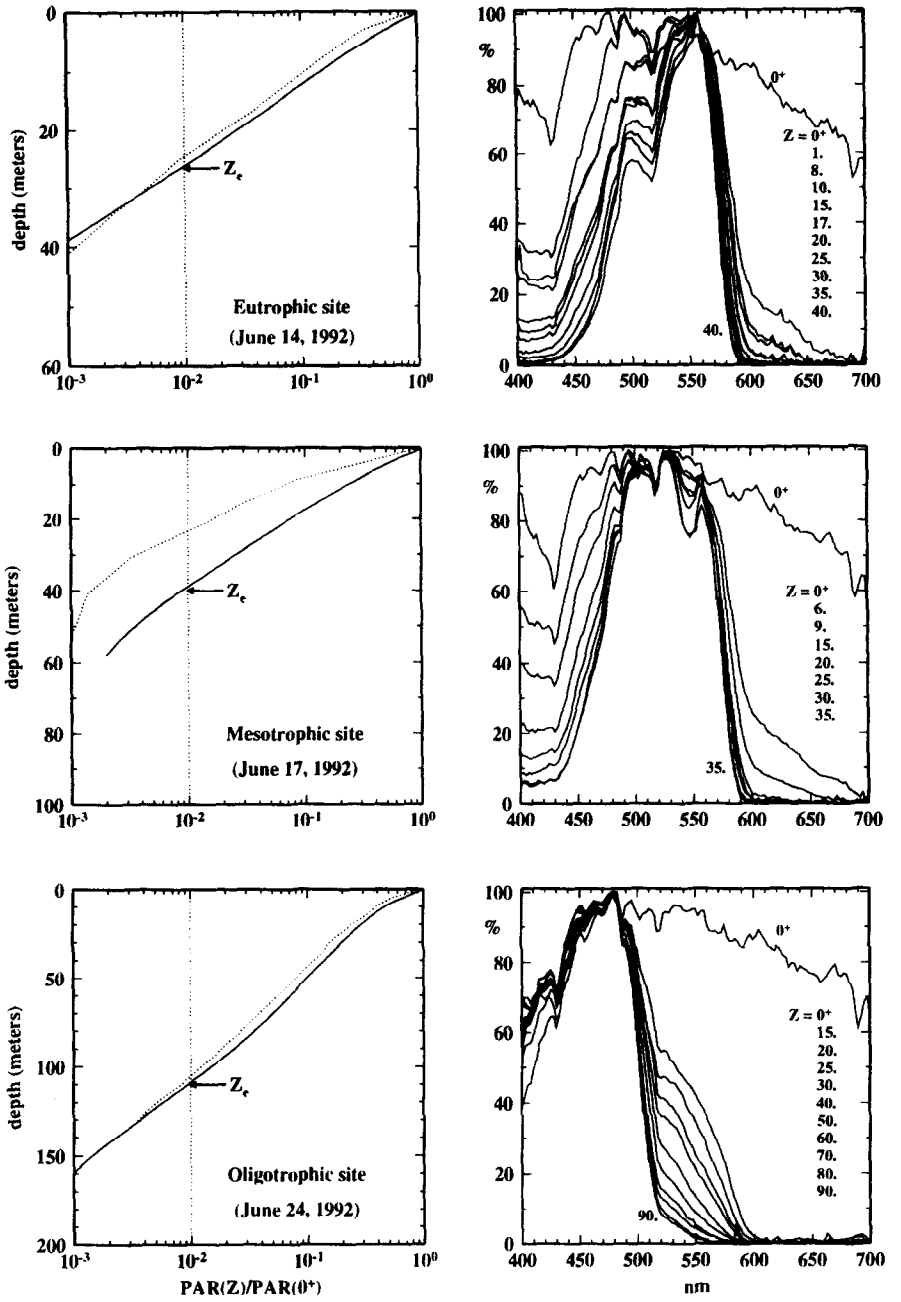

Fig. 4. Vertical profiles (left panels) of the photosynthetically available radiation, PAR(z), normalized to the surface value, PAR(0^+); the solid curves represent the profiles computed from the vertical Chl distribution (Morel, 1988), whereas the dotted curves are from measured values. Spectral distributions (right panels) of the downwelling irradiance in relative units (each spectrum normalized to its maximum value) and for various depths (0^+ means "above surface"). The three rows are for the three sites.

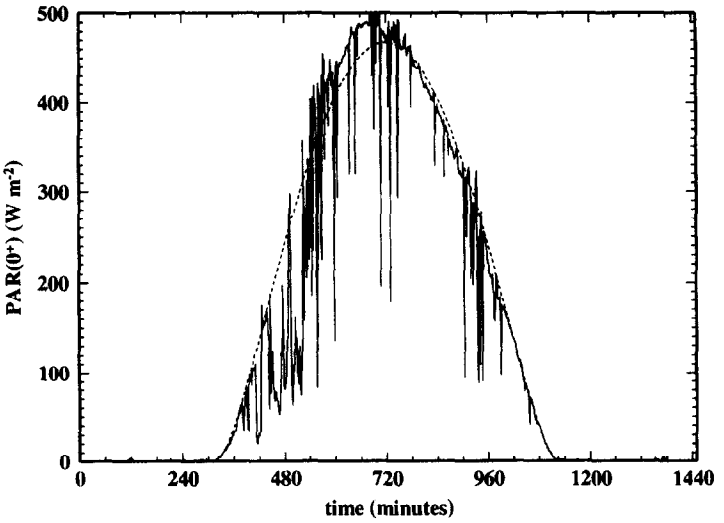

Fig. 5. Daily cycle of the photosynthetically available radiation incident at the surface, PAR(0^+). The solid curve is derived from the pyranometer (Eppley) records, averaged over 1-min periods, and simply multiplied by the factor 0.43 (Jitts *et al.*, 1976). The dotted curve is produced by the standard model (see text) for a cloudless atmosphere at the same latitude (21°N) and for the same day (22 June) and with standard values for atmospheric parameters (ozone: 350 DU, water vapor: 2 cm of precipitable water, aerosol of "marine type", visibility: 23 km).

Fig. 5); this capacity will not be used here (except for sensitivy analyses; see later on). Through its bio-optical segment (used here), the model predicts, for Case 1 waters only, the propagation of radiation throughout the water column, as well as the changes in spectral composition as governed by the Chl(z) profile. The productive column actually considered has a thickness $Z_p = 1.5\ Z_{eu}$, where Z_{eu} represents the euphotic depth commonly defined as the depth where PAR is reduced to 1% of its surface value; the depth increment for all computations is $Z_p/100$.

In the model, when operated in its standard version, parameters of algal physiology are fixed and constant whatever the depth. The shape of the algal absorption spectrum, its maximum value at 440 nm, denoted a^*_{max}, the maximum quantum yield for growth, $\varphi_{\mu max}$, and KPUR, the normalizing irradiance (related to E_k and sizing P^B_{max}; see the Appendix, equation (A8)) are given prescribed values (version 1 in Tables 1 and 2). KPUR is allowed to vary with temperature with a Q10 factor of 1.88 as in Eppley (1972); this factor represents the relative increase in light-saturated photosynthesis rate for a 10°C temperature increase. The photosynthesis light response is optionally modeled according to various mathematical representations. For consistency with the fitting procedure applied to the P versus E curves, the hyperbolic tangent function is selected for all following computations. Note that a "version 2" of the standard model will be introduced later (in the Discussion) and is not used here; it differs from "version 1" only by the different values given to the photo-physiological parameters.

When specific information on the absorption and photosynthetic responses of algae are available, as was the case here, the model can be operated in an "adjusted" mode, where the standard characteristics are replaced by the actual and depth-varying values of a^*_{max}, $\varphi_{\mu max}$, and KPUR (as shown in Figs 6–8). Interpolations between sampling depths are performed

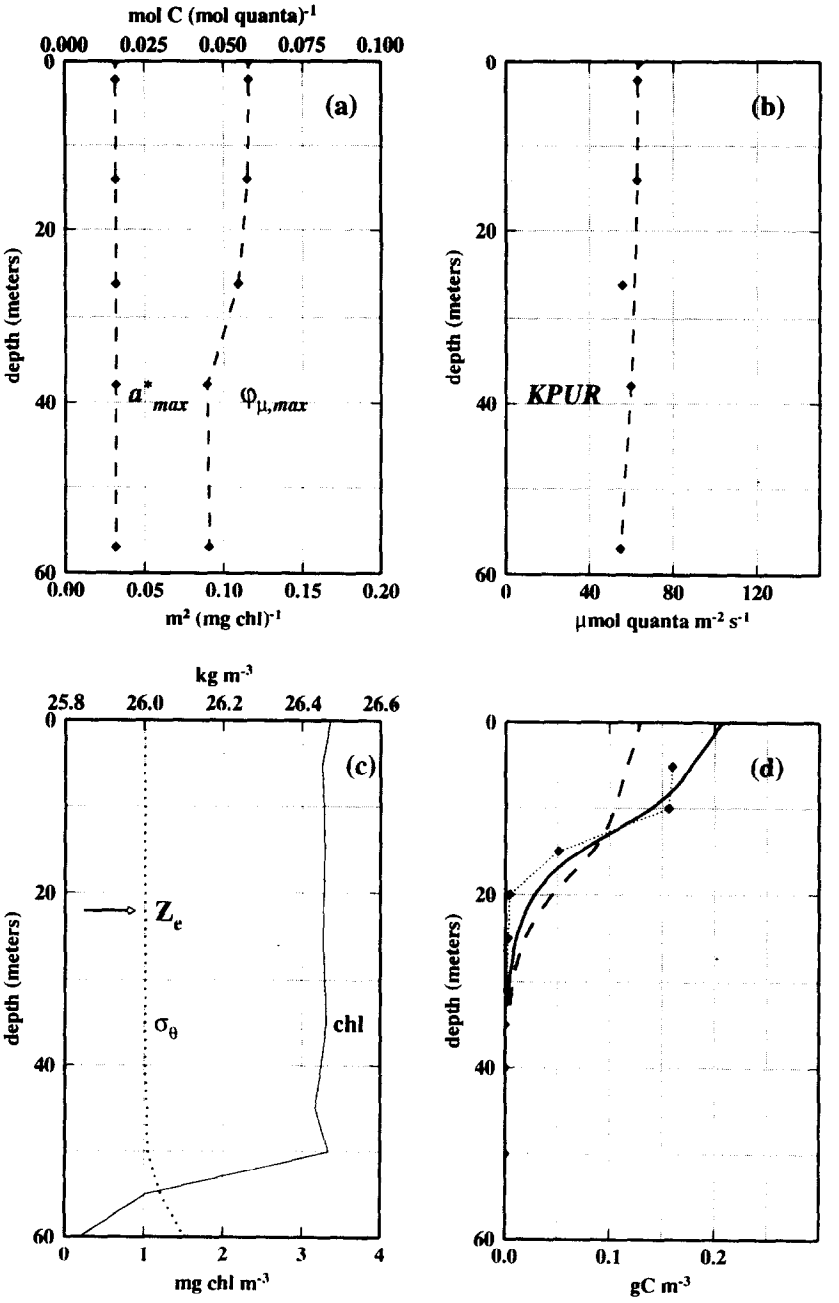

Fig. 6. As a function of depth are plotted the mean bio-optical (a^*_{max}) and physiological parameters ($\varphi_{\mu max}$ and KPUR, see text) determined at the eutrophic site; the standard errors for these profiles are displayed in Babin *et al.* (1996). The Chl(z) profile is shown together with the density excess profile (σ_θ), for 13 June 1992. The last panel displays the primary production vertical profiles, as measured (13 June 1992, diamonds), and as computed from either the standard model version 1 (dashed curve) or the adjusted model (solid curve).

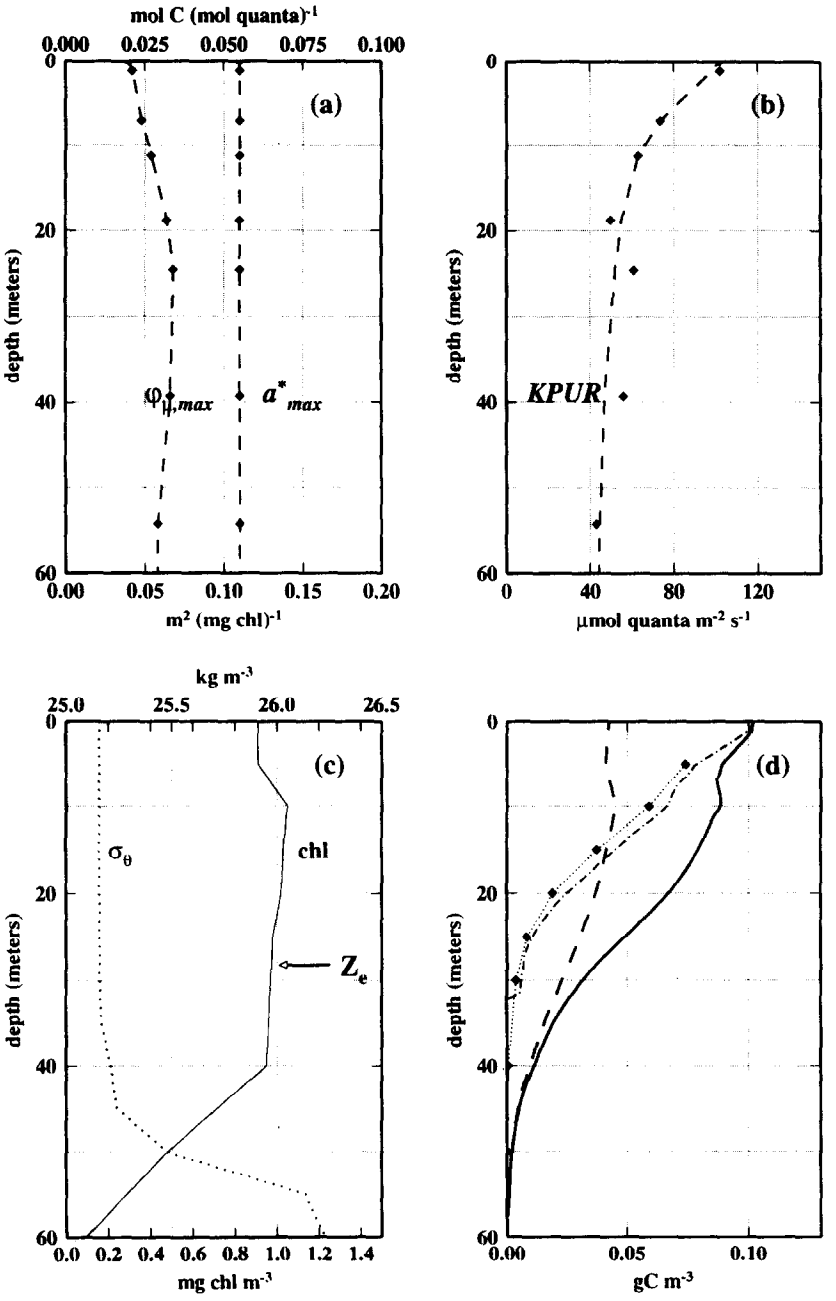

Fig. 7. As in Fig. 6, but for the mesotrophic site (17 June 1992); note the dotted–dashed curve in panel (d) which represents the production profile computed from the adjusted model combined with the actual light profile at this station (see Fig. 4).

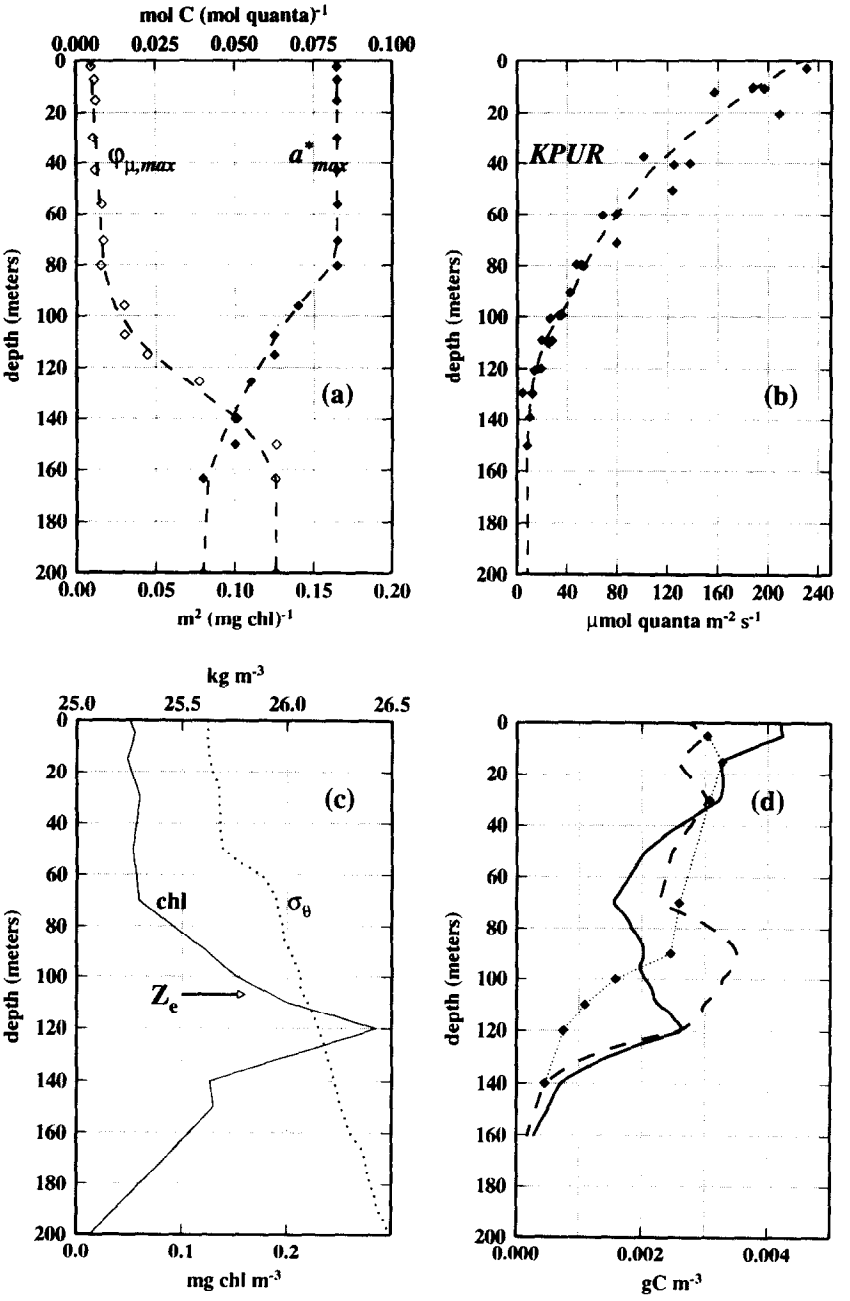

Fig. 8. As in Fig. 6, but for the oligotrophic site (22 June 1992). Note here that the KPUR vertical profile was fitted onto individual determinations rather than onto the mean values presented in Babin *et al.* (1996).

for Chl(z) and physiological parameters as required by the adopted depth-increment, so that the standard and adjusted models differ only by the use of different parameters, but not in their vertical resolution. In a similar way, the diurnal course of PAR (0^+), as recorded at the surface, is introduced with daylength/60 as increment in the standard and adjusted computations.

RESULTS

The vertical profiles of α^B and P^B_{max} and a detailed examination of the inter- and intra-site variability of the photosynthetic parameters are given in Babin *et al.* (1996). We summarize here these results, in the specific context of primary production modeling, with particular reference to the quantities, such as $\varphi_{\mu max}$, KPUR and a^*_{max}, that are needed to operate the "adjusted" model. This adjusted model, in essence, extends and refines early attempts at estimating primary production from P versus E characteristics in combination with available photosynthetic irradiance (see e.g. Fee, 1973; Jitts *et al.*, 1976; Côté and Platt, 1984; Harrison *et al.*, 1985). The standard model is used only in its version 1 in what follows.

Eutrophic site

At this location, the mixed layer ($Z_{ml} \cong 50$ m, temperature $T = 17.8°C$) extends deeper than does the euphotic layer ($Z_{eu} \cong 20$–25 m). With a quasi-uniform Chl(z) profile and concentrations averaging 3 mg m^{-3}, the well mixed algal population exhibits essentially constant optical and physiological characteristics throughout the water column (see Fig. 6). The rather low a^*_{max} value is typical of diatoms, predominant in this upwelling area. The $\varphi_{\mu max}$ values, about 0.06 mol C (mol quanta)$^{-1}$, are close to the one used in the standard computation [0.07 mol C (mol quanta)$^{-1}$] adopted from Bannister and Weidemann (1984). To the extent that KPUR (as well as a^*_{max} and $\varphi_{\mu max}$) remain constant regardless of depth in the mixed layer, it appears that vertical mixing rates are faster than photoadaptative responses of algae (Lewis *et al.*, 1984). In such a case, the global response of the algal community results in a photoacclimation to the mean irradiance within the mixed layer (actually amounting to 9.3% of the surface irradiance; see in Babin *et al.*, 1996). It is worth noting that the field value of KPUR is about twice that adopted in the standard set of parameters (version 1, Tables 1 and 2).

Figure 6(d) shows the measured *in situ* primary production profile and those computed from the Chl(z) profile, with either the standard or the actual values for the photophysiological parameters (see Tables 1 and 2). For the upper layer, the standard model predicts carbon fixation values lower than field values. At shallow depths, the production rate is light-saturated during the main part of the light period. As the selected standard KPUR and therefore P^B_{max} values are lower than the field values [3.41 versus 5.5 g C (g Chl)$^{-1}$ h^{-1}], the resulting computed production is also too low. With the actual KPUR values, the adjusted model produces results in agreement with *in situ* determinations. A deeper, light-limited photosynthesis regime prevails during the day, so that the initial slope α'^B (cf. the Appendix) becomes the determining factor. Because the standard α'^B value is set above the actual one [37.8 versus 21.1 m^2 g C (g Chl)$^{-1}$ (mol quanta m^{-2})$^{-1}$], the modeled production exceeds the measured one in the vicinity of Z_{eu}. In spite of these divergences, the computed daily areal productions are not far from those measured (Table 3). For all depths, the adjusted model provides improved estimates (Fig. 6(d)); the column

integrated carbon fixation resulting from the computed production profiles (using the adjusted model) are slightly above those derived from the *in situ* determinations (Table 3). The trapezoidal integration, and the extrapolation toward the surface of the single production values measured at 5 m, explain most of the difference between the actual column production and the computed one (using a depth increment of 0.3 m).

During the first leg of this cruise, the *in situ* primary production was measured without parallel *in vitro* determinations of $a^*(\lambda)$ and P versus E curves. The chlorophyll was also uniformly distributed along the vertical, but was much lower ($1.4\,mg\,m^{-3}$). If the physiological parameters determined 8 days later are combined with this Chl(z) profile, the computed primary production profile, as well as the integrated value, still agree with the *in situ* determinations (Table 3 and Fig. 10(a)).

Mesotrophic site

At this site, the mixed layer thickness again exceeded that of the euphotic zone (40 m versus 27 m, on average) and the mean irradiance in the mixed layer amounted to 16% of the surface irradiance. With Chl(z) slightly above $1\,mg\,m^{-3}$ (from 0 to 20 m) the algal standing stock remained essentially constant over 3 days. Somewhat surprising was the predominance of cyanobacteria within this rather dense algal population, as attested by the phycoerythrin absorption band distinctly seen in all algal absorption spectra (see Babin *et al.*, 1996) or in the downwelling irradiance spectra (dip around 547 nm; Fig. 4). This predominance is also confirmed by cell enumeration (Partensky *et al.*, 1996). The a^*_{max} value at 437 nm, almost constant with depth (Fig. 7(a) and Tables 1 and 2), was high [$\cong 0.11\,m^2\,(mg\,Chl)^{-1}$]. The yield, $\varphi_{\mu max}$, was weakly varying between 0.02 and 0.03 mol C $(mol\,quanta)^{-1}$, whereas the KPUR profile showed a slightly decreasing slope from the surface downward. The near surface KPUR value was about three times larger than the selected standard value; even near Z_{eu}, the actual KPUR remained twice the standard one.

As expected from such a divergence in the KPUR values and therefrom in P^B_{max} (Tables 1 and 2), the realized production in the upper 15 m layer was notably underestimated through the standard computation (Fig. 7(d)). Surprisingly, the adjusted model did not provide better estimations, except near the surface. Below 20 m, both models strongly overestimated the light-limited production.

The reason for this discrepancy was not in the model formulation nor in the parameters values; it lies in the "anomalous" optical properties at this location. The actual PAR(z) profiles (one example shown in Fig. 4) markedly differ from those generated from the Chl(z) profiles and the bio-optical model developed for nominal Case 1 waters. The algal assemblage dominated by *Synechococcus* and associated retinue is likely at the origin of such a departure. If the measured spectral distributions and PAR(z) values are used in place of the modeled ones, the production profiles computed with the adjusted model give excellent agreement with the field data (Fig. 7(d) and Table 3 for the column integrated productions during the 3 days at this site).

During the first leg, the biomass was similarly distributed but with a lower concentration (about $0.5\,mg\,Chl\,m^{-3}$ from 0 down to 40 m). Entering the physiological parameters measured during the second leg (i.e. 15 days later) into the model led to an overestimate of the measured production during the first leg, particularly below 20 m (Fig. 10(b)). This divergence, similar to that already noted for the second leg, suggests (by analogy) an abnormally enhanced light absorption in these waters.

Oligotrophic site

Compared to those at the two other sites, the physical conditions at the oligotrophic site are reversed, as the euphotic zone (Z_{eu} about 105 m) extends much deeper than the mixed layer (Z_{ml} about 60 m, on average, Fig. 8(c)). The mean irradiance in the mixed layer amounts to 33% of the surface irradiance. Fluctuations in Z_{ml}, at least of ± 10 m, were observed during the 6 days spent at this site. They originate from internal waves, which also affect the position of the permanent and well developed deep chlorophyll maximum (DCM). The peak in biomass (about 0.3 mg Chl m^{-3}), oscillating around 125 m by ± 20 m, actually is stable with respect to the density profile and centered around $\sigma = 26.15$ (see Fig. 9). The structure of the algal assemblage, dominated by picoplanktonic species (*Prochlorococcus*, *Synechococcus* and pico-eukaryotes), evolves progressively with depth, as does the pigment composition (Partensky *et al.*, 1996; Claustre and Marty, 1995). The bio-optical and physiological properties of these algae also vary with depth, in particular through the pycnocline (Fig. 8(a) and 8(b)).

The Chl-specific absorption coefficient was constant within the mixed layer, with very high values mainly due to the significant proportion of zeaxanthin in the pigment composition of these cells. Below this layer, a^*_{max} regularly decreases. From extremely low values within the mixed layer, where zeaxanthin does not act as a photosynthetic pigment (see the Appendix), the maximum quantum yield progressively increased throughout the DCM and reached high values at the deepest levels. The smooth decrease of KPUR (or

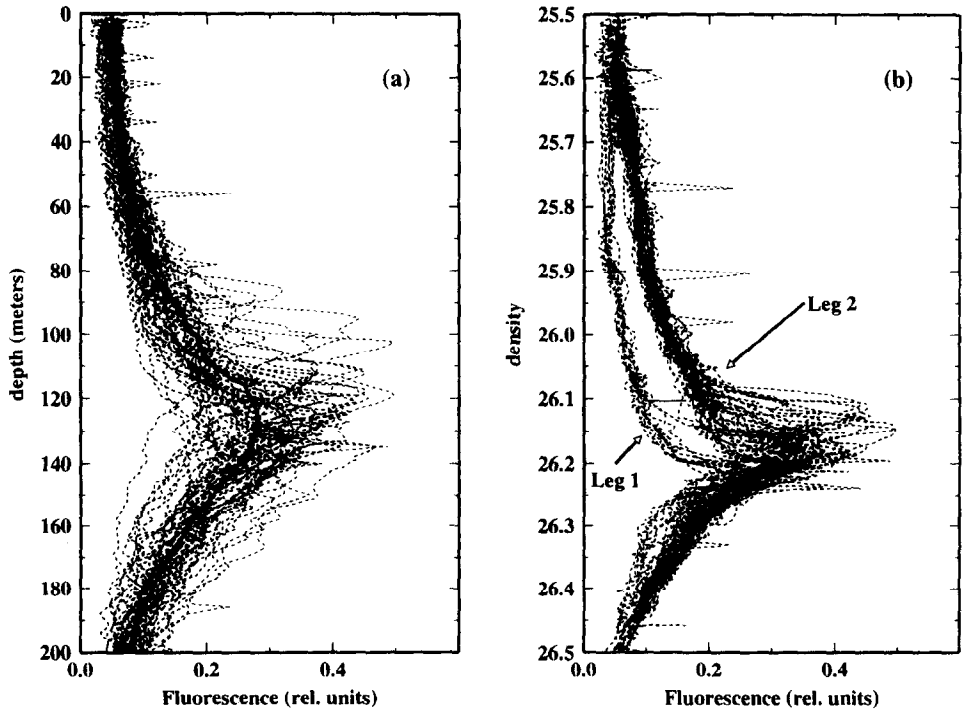

Fig. 9. Chlorophyll fluorescence vertical profiles at the oligotrophic site. The data of the two legs of cruise 4 are pooled together [panel (a)]. In panel (b), the same profiles are plotted as a function of density excess.

equivalently of P^{B}_{max}) between 0 and 80 m tends to demonstrate that the population inside the mixed layer is not actively mixed but rather is able to undergo some photoacclimation to the local prevailing irradiance. Extremely low KPUR values characterized the deep photoadapted population in the stratified layers (at the DCM level and below).

The comparison of the actual and computed primary production profiles (example in Fig. 8(d)) showed that there was an overall agreement at least for the mixed layer. The grossly similar outputs of the standard and adjusted models, however, result from somewhat fortuitous and compensatory effects. Experimental values of α_{max}, $\varphi_{\mu max}$ and KPUR are strongly variable and differ from the standard values (Tables 1 and 2). Nevertheless, their combination through equations (A2b) and (A8) (Appendix) results in light-saturated production rates close to the single P^{B}_{max} value that was adopted in the standard model. The light-saturated production value is essential for the upper layer production. Below, both models predict a maximum of production centered (adjusted model) or above (standard model) the DCM, whereas such a maximum does not appear distinctly in the measured primary production profiles. A careful examination of the actual and standard α'^{B} values provides the clue for explaining the difference between the two models, but not the difference between the model outputs and the measurements. This will be examined later (see Discussion).

At the oligotrophic site, the results obtained during the first leg (4 weeks before leg 2) were practically identical in terms of algal biomass, algal composition and primary production. The results of the two legs are therefore pooled together (Fig. 10(c)) for comparison with the modeled values. In such oligotrophic waters, with low production rates, the *in situ* data are somewhat noisy; in addition, the situation was complicated by internal waves, which move the DCM upward or downward. Both the standard and adjusted models have in common an overestimation of primary production measured at and below the DCM, and the standard model results in greater production from the intermediate level (60 m) downward. Except for the 25th of May, the measured and predicted column-integrated values (Table 3) agree well (within $\pm 10\%$), partly because over- and underestimates compensate.

The validation of the standard and adjusted models can be extended to the primary production data obtained 8 months earlier at the mesotrophic and oligotrophic sites during EUMELI no. 3 (the eutrophic site was not visited during this cruise).

Using EUMELI-3 as a test data set

At the mesotrophic site, the situation differed from that found eight months later. The algal biomass within the euphotic layer was much lower (about 1/3), and a DCM was developed around Z_{eu}, at 40 m, below a nutrient-depleted mixed layer (20 m thick). Such Chl(z) profiles tend to resemble those typical of oligotrophic situations. The standard model overestimated the carbon fixation, in particular at the DCM level (integrated values in Table 3). The adjusted model, not surprisingly, yielded under-estimates for all depths because the parameters determined during EUMELI no. 4, for this particular community living in an extended mixed layer, did not reflect the physiological status of the algal community established in the highly stratified column set up in September.

In contrast, the situation at the oligotrophic site was basically the same in October and in June in terms of algal biomass, pigment composition (Claustre and Marty, 1995) and layering of phytoplankton assemblages (Partensky *et al.*, 1996). The standard and adjusted computations provided the same kind of agreement (or of divergence) with the EUMELI

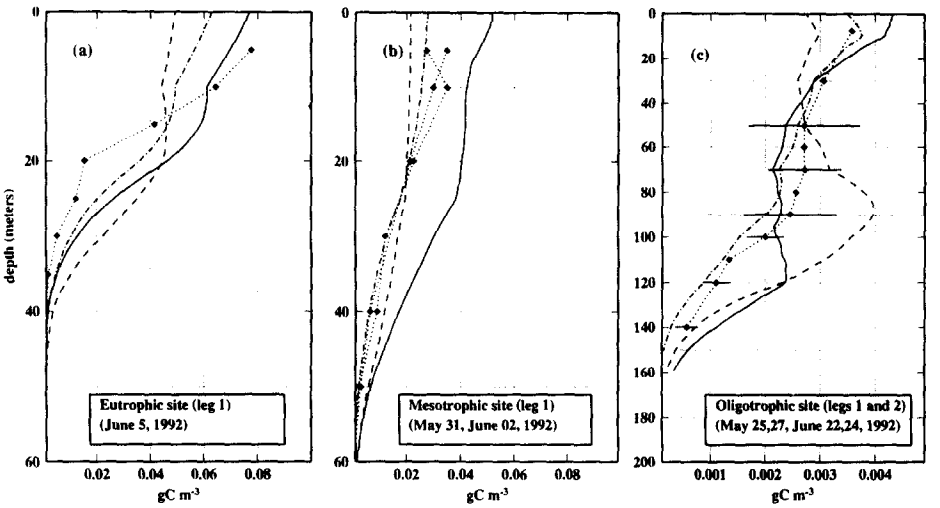

Fig. 10. Primary production profiles as measured (diamonds) or computed according to the standard (version 1), or to the adjusted model (dashed and solid curves, respectively). Leg 1 (cruise 4) data for the eutrophic and mesotrophic sites are compared to modeled profiles by using the physiological parameters measured during leg 2. For the oligotrophic site, the data of legs 1 and 2 have been averaged and the horizontal bars are for one SD; the computations are made using an averaged (legs 1 and 2) Chl(z) profile. In the three panels the dashed–dotted curves are produced by the standard model in its version 2 (see text).

no. 3 *in situ* measurements as previously noted with those of EUMELI no. 4. The adjusted model worked rather well, while the standard one produced values that were too high, especially at the intermediate levels and within the DCM (see profiles in Fig. 11). In terms of column integrated production, both the adjusted and standard computations led to values exceeding the field values (by 38 and 73%, respectively; Table 3).

DISCUSSION

Model efficacy

Compared to the standard model version 1, the adjusted model provides production profiles closer to, but not coinciding with, the actual profiles (Fig. 12). Besides the fact that *in situ* and *in vitro* determination of carbon fixation are not error free, perfect agreement between modeled and measured values is improbable. In reality, the physiological parameters determined during short incubation periods (about 2–3 h) cannot in essence account for the *in situ*, nearly net, carbon fixation measured over a 24 h period (Harrison *et al.*, 1985; Cullen *et al.*, 1992b). A long incubation experiment involves a composite of photosynthetic performances (see e.g. Henley, 1993) and also sums up processes other than photosynthesis. The notable exception to overall agreement between measured values and those computed with the adjusted model, was found in mesotrophic waters and originates from an inadequate representation of the light propagation in these waters rather than from the use of inappropriate physiological parameters. The model can also cope with various trophic regimes and production values that span more than two orders of magnitude (Fig. 12).

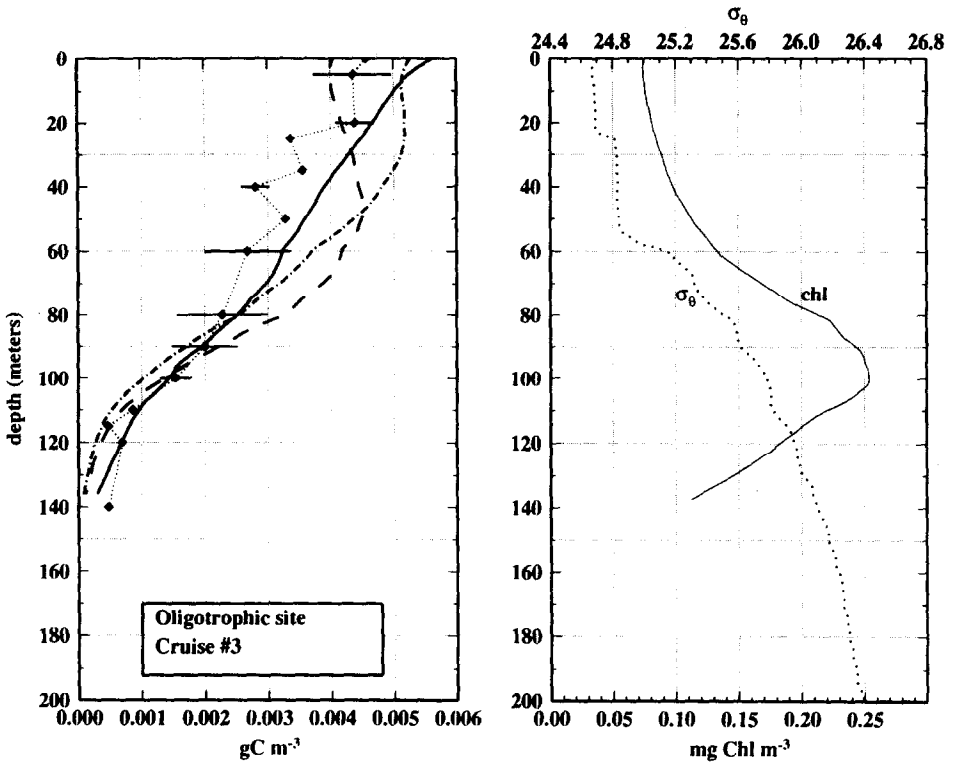

Fig. 11. As in Fig. 10 but for the oligotrophic site only and data of the EUMELI cruise 3 (data for 18 and 20 October excluded from the averages). The mean Chl profile for this cruise used for the computation, is also shown, together with the density excess profile of 16 October 1991.

The constant standard physiological parameters for version 1, were somewhat subjective, reasonable means of *in vitro* or *in situ* values (see Morel, 1991); through a validation exercise (Berthon and Morel, 1992), this choice was confirmed to the extent that no significant bias in terms of integrated production resulted from its use. For these reasons, the standard model generally provides reasonable estimates when operated (hindcast) for the 17 stations of cruises 3 and 4 (Table 3); it results in a slight overestimate of the integrated production (by 25%, on average), with a standard deviation of 35%. In contrast, the vertical profiles of carbon fixation are not well reproduced with this version 1. As a rule, an underestimate relative to the actual values is systematically produced by the model in the upper layer, whereas an overestimation appears deeper; the two roughly compensate each other. These discrepancies and their causes are examined below by separate analysis of the effect of the various parameters involved in the computation.

Sensitivity studies related to photo-physiological parameters and incident irradiance

Two independent parameters, a^*_{max} and $\varphi_{\mu max}$ (Appendix), are combined through their product to determine the initial slope, α'^B, which characterizes the light-limited carbon fixation rate. The enzyme controlled, light independent, maximum rate is described by the single parameter P^B_{max} (KPUR is a derived parameter through the ratio P^B_{max}/α'^B). These

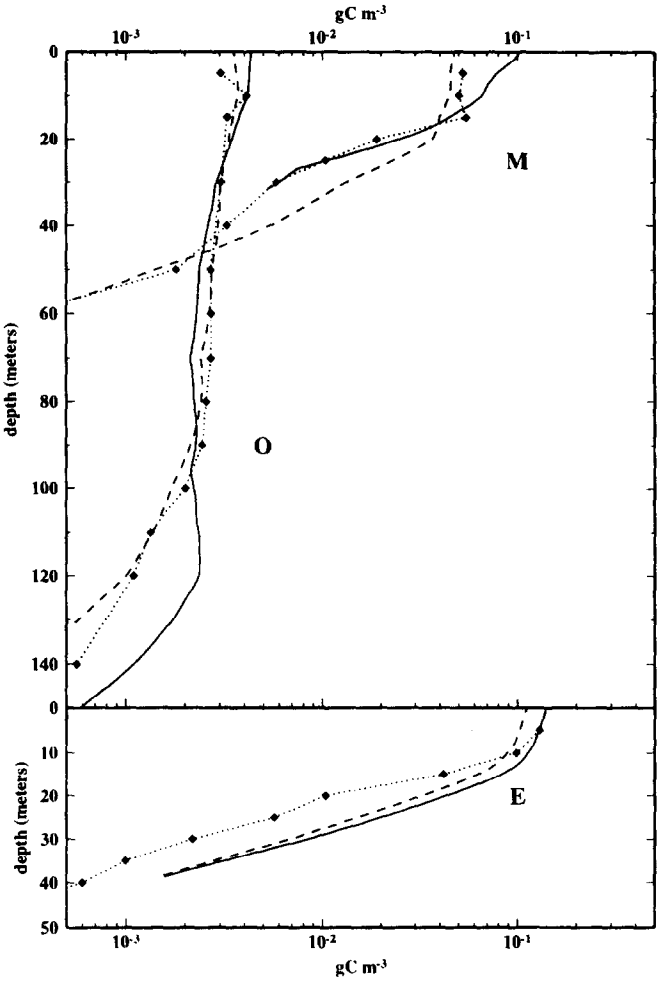

Fig. 12. Primary production values (logarithmic scale) measured and averaged at each of the three sites. Leg 1 and 2 data (EUMELI 4) are pooled together and averaged (diamonds). The computed profiles make use of averaged Chl(z) profiles for each site; solid curve: adjusted model; dashed curve: standard model, version 2.

two descriptors of the P versus E curve, which pertain to two distinct mechanisms (light and dark reactions), are physiologically and mathematically independent. Nevertheless photoacclimation (e.g. Geider *et al.*, 1993) often results in concomitant, generally opposite, variations in both. For the oligotrophic site, the evolution of the P–E curves with increasing depth (Fig. 3) clearly shows the simultaneous increase in the initial slope and the lowering of the plateau. These converse variations cause a dramatic change in E_K or KPUR with depth (Fig. 8(b)).

$P^B{}_{max}$ and α'^B have a distinct impact upon the column integrated production. Within the upper layer of the productive column, carbon fixation is expected to reach its ceiling value during a sizable part of the day, while in the deeper dimly-lit layers, the value of the initial slope presumably is the permanent governing factor. The production realized at such deep levels, however, contributes only a minor part of the entire column production, so that

P^B_{max} might be considered as the most influential parameter, as far as integrated production is concerned.

The relative effect of both these parameters on daily areal production has been examined by Lewis *et al.* (1985). This analysis deals with a simple case allowing partial derivatives to be made explicit; the simplifying assumptions are as follows: constant insolation and PAR attenuance, uniform chlorophyll distribution and photosynthesis parameters throughout the water column. Taking into account the varying surface irradiance during the day, and considering a more realistic PAR propagation, with its spectral composition, as well as the vertical variations in the physiological parameters, impedes a simple mathematical analysis. Numerical experiments, conversely, are easy and can allow the photic zone to be partitioned into a "light-saturated layer" and a "light-limited layer" (Bienfang *et al.*, 1984). The respective roles of P^B_{max} and α'^B in the *in situ* carbon fixation process can therefore be assessed.

Three particular days at the three sites are considered, with their specific PAR irradiance and the mean depth-dependent physiological parameters. The isolines of the ratio PUR to KPUR are shown as a function of time and depth in Fig. 13. The two regimes (light-saturated and light-limited) are delineated by the isoline corresponding to unity. At the well-mixed eutrophic site, KPUR and P^B_{max} are constant with depth. Acclimated to the rather low mean irradiance level prevailing in the mixed layer, the algal population cannot take advantage of the light availability in the upper, well-lit layers. The light-saturated regime (i.e. when PUR > KPUR) dominates during two thirds of the day, and within about half of the euphotic zone. The production realized in the light-independent, saturated regime represents 68% of the total column production. At the oligotrophic site, in contrast, a vertically structured photoacclimation occurs (Fig. 8(a) and (b)), which tends to enhance the role of α'^B at the expense of that of P^B_{max}. The carbon fixation effected in the light-saturated mode is accordingly lowered (48% of the total fixation for the whole day); meanwhile 52% is realized under light limitation. The mesotrophic situation is roughly similar to that at the eutrophic site, with 70% of the production realized under saturation, although the PUR-to-KPUR ratio does not reach (near the surface) values as high as those observed at the eutrophic site.

The partitioning described above is expected to change if the same population (with the same physiological state) is exposed to differing PAR conditions (the temperature is left unchanged). These changes are displayed in Fig. 14 for the three sites. The PAR values computed for the 1st of June, at latitude 20°N and with a cloudless sky of medium visibility (23 km), are used as reference. Interestingly, the relative contribution of production in the light-limited regime to the total column production changes only slightly, i.e. increases slowly, when the incident irradiation diminishes (at least, as long as it remains above half the reference value). Below this threshold, the changes are more accentuated, in particular at the oligotrophic site, where as seen above, the light-limited regime was already prevalent even at high irradiance. As previously demonstrated (Fig. 21 in Morel, 1991), the integrated production decreases in a non-linear manner with decreasing incident irradiation. When PAR is halved, for instance, the areal production still amounts to 77%, 80% and 65% of its initial value at the eutrophic, mesotrophic and oligotrophic sites, respectively. It is worth emphasizing that the above numerical predictions are made under the assumption of neither photoacclimation nor photoadaptation (species succession) to the imposed insolation conditions. In the natural environment, the predicted trends are likely couterbalanced, at least partly, as soon as adaptation starts to occur.

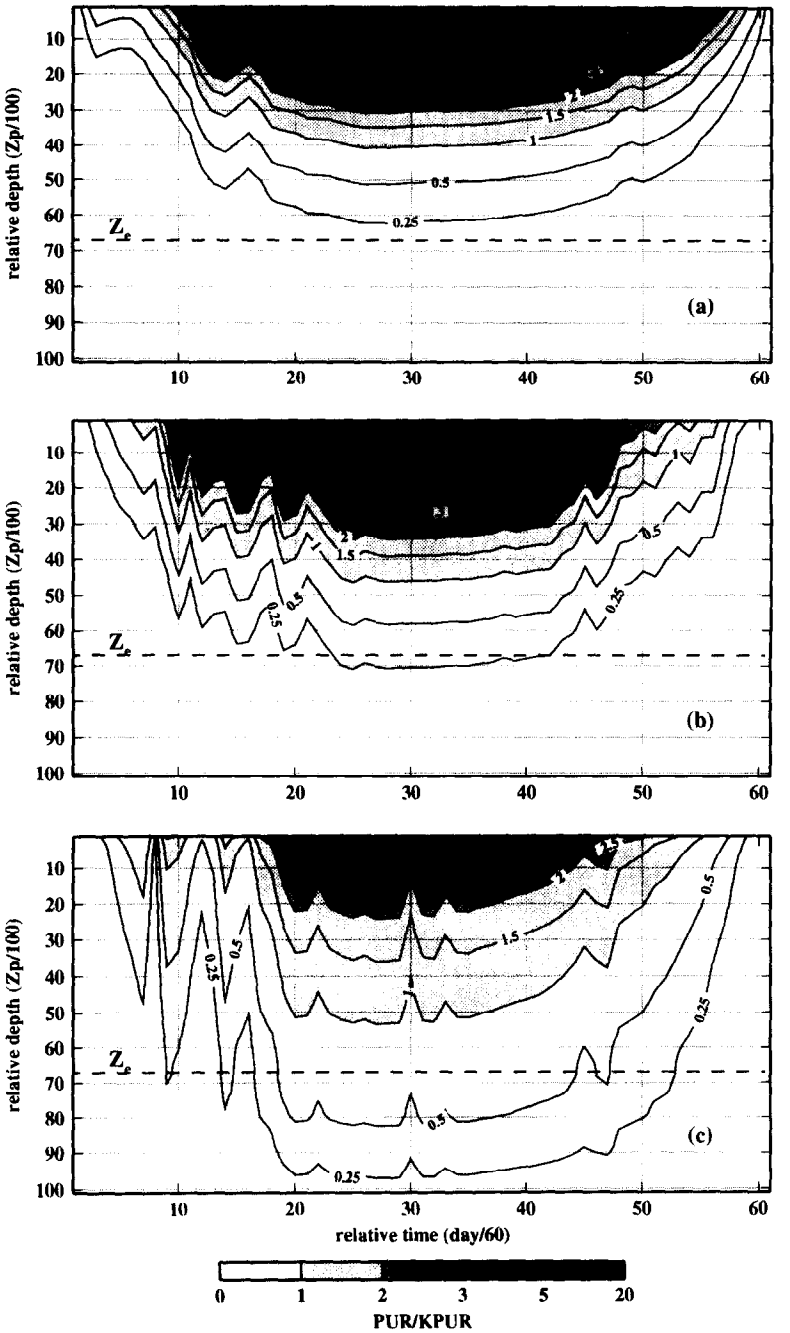

Fig. 13. Isopleths of the ratio PUR/KPUR as a function of the time (increment daylength/60) and of the depth (increment $Z_p/100$). The irradiance recorded at the surface and the KPUR values derived from P versus E measurements are used to draw these graphs. Irregular patterns are the result of clouds occurrence. (a) Eutrophic site, 13 June 1992. (b) Mesotrophic site, 17 June 1992. (c) Oligotrophic site, 22 June 1992.

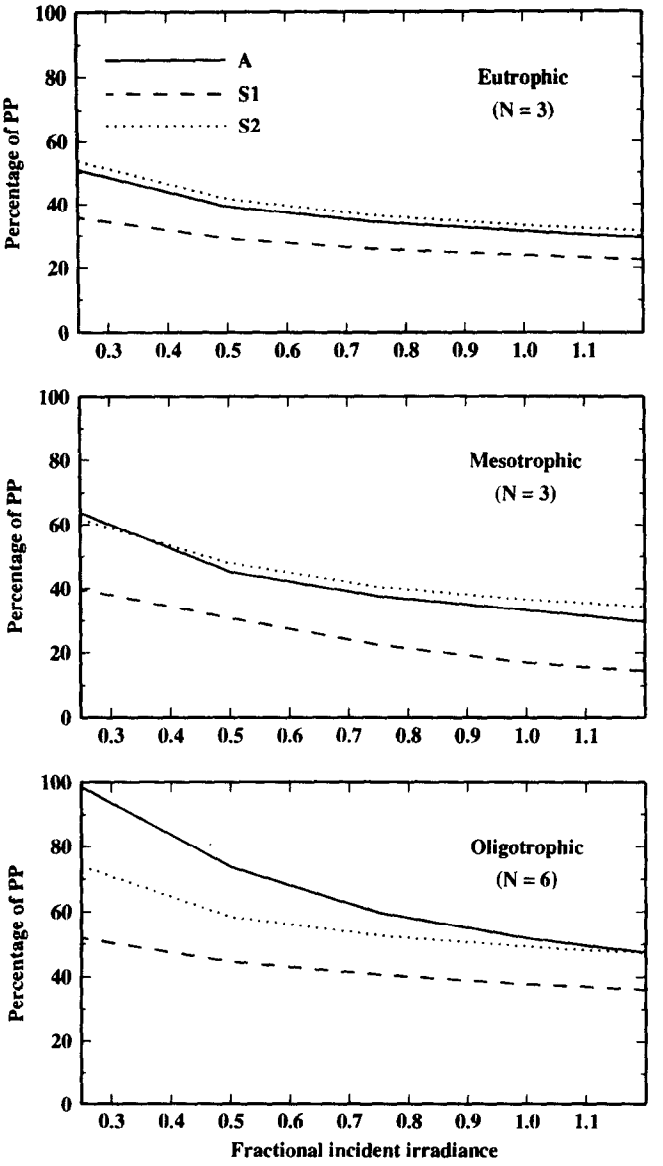

Fig. 14. Fraction of the column production (as %) realized in the light-limited layer (where PUR < KPUR), as a function of incident irradiance, expressed in relative units (with respect to a reference value, see text). Solid curves (label A) are computed using the adjusted model; dashed and dotted (label S-1 and S-2) are computed using the standard model, version 1 or 2. The computations corresponding to successive (N) days at each site are averaged to produce single curves; the individual curves for each day do not differ from the corresponding (A, S-1 or S-2) mean curves by more than 2%.

To complement the above analysis, another kind of numerical experiment can be carried out by retaining the actual irradiance conditions and changing the physiological parameters. With this purpose, the 12 stations of EUMELI 4 are considered. In a first experiment, P^B_{max} is allowed to double with respect to its initial (depth dependent) value while the initial slopes are kept unchanged; these slopes are doubled in a second experiment, while P^B_{max} is unchanged; finally, in a control experiment, both parameters are simultaneously doubled, leading (as verified) to an exact doubling of the integrated production. The relative increases in integrated production, $\Delta P/P$, for the three trophic regimes are provided in Table 4. As expected from the results concerning the predominance of the light-saturated regime at the eutrophic and mesotrophic sites, doubling P^B_{max} has more influence on P (increased by about 53%), compared to a doubling in α'^B (resulting in an increase in P by about 23%). The respective impacts of the two parameters are more balanced at the oligotrophic site, where, as already noted, the light-limited production accounts for at least half of the total production (Fig. 14). According to the study by Lewis *et al.* (1985), P^B_{max} would have, in general, less effect on the column production than the initial slope; actually, these authors discuss the effect of experimental "errors" in the photosynthetic parameters on estimates of integrated production; their statement, however, can be repeated in terms of "changes" in place of "errors". The present analysis leads to the conclusion that such a simple statement on the dominant role played by P^B_{max} is risky if generalized. The situation is more complex and any conclusion depends on the respective values of the two parameters, on their vertical distribution, and ultimately on surface irradiance, which, in turn, may entail a shift of the photo-physiological parameters through photoacclimation or photoadaptation.

Improving standard models

Using adjusted models with the pertinent parameters for a given time and place would be the ideal solution for a meaningful exploitation of the remotely sensed pigment biomass at all scales; for that, however, much more information on the vertical distribution of the P–E curve parameters and on their regional and temporal variability is clearly needed.

Table 4. Mean values of the relative change in column primary production ($\Delta P/P$ *as %*) *when* (1) P^B_{max} *is multiplied by* 2, α'^B *left unchanged, or conversely* (2) *when* α'^B *is doubled with* P^B_{max} *unchanged; AM : computed with the adjusted model and actual depth-varying physiological parameters; SM-1 and SM-2 : computed with the standard model, versions* 1 *and* 2, *and constant physiological parameters given in Table* 1

	AM		SM-2		SM-1	
Site	(1) $P^B_{max} \times 2$	(2) $\alpha'^B \times 2$	(1) $P^B_{max} \times 2$	(2) $\alpha'^B \times 2$	(1) $P^B_{max} \times 2$	(2) $\alpha'^B \times 2$
Eutrophic ($N=3$)	+52.2	+25.2	+50.0	+26.7	+62.2	+19.0
Mesotrophic ($N=5$)	+53.1	+20.8	+47.0	+25.8	+60.0	+14.6
Oligotrophic ($N=6$)	+28.4	+37.5	+35.6	+40.0	+47.9	+29.3

Therefore, until such data are available, it will remain necessary to rely on a standard model, or whenever possible, on some locally adapted versions of this model for a variety of biogeochemical provinces (Platt and Sathyendranath, 1988).

In the standard model, version 1, the adoption of a KPUR value that is too low (and consequently of P^{B}_{max} values that are too low) shifts the production toward the light-saturated regime in an unrealistic manner. In the same vein, doubling P^{B}_{max} has more impact on P if this standard model is used, instead of the adjusted model (see columns "SM-1" in Table 4). Therefore a desirable modification would be to adopt a higher KPUR value and a smaller α'^{B} value, in order to globally preserve the resulting integrated production. Some guidance along these lines can be found in recently published results, examined hereafter.

Empirical relationships describing the evolution of several photo-physiological parameters with the trophic status of oceanic waters have emerged since the standard set (version 1) of parameters was selected, and they can be used for modifying this previous set. It has recently become clear that the Chl-specific absorption of algae does not vary at random; rather it shifts regularly with the chlorophyll concentration in oceanic waters (Wozniak and Ostrowska, 1990; Bricaud *et al.*, 1995; Carder *et al.*, 1991; Cleveland, 1995). Maximal a^* values are found in oligotrophic waters (predominance of tiny cells with high carotenoid content) and minimal values in eutrophic waters (large cells, lower accessory pigments content). A discussion of the pigment compositions in different trophic regimes can be found in Claustre (1994). The Chl-specific absorption values used in the present study follow this general pattern (Fig. 3 in Babin *et al.*, 1996). Conversely, from low values in nutrient depleted waters, the maximum quantum yield tends to increase in a more favorable environment (Falkowski *et al.*, 1991; Geider *et al.*, 1993) in such a way that $\varphi_{\mu max}$ would roughly parallel the level of biomass itself. These opposite trends in a^*_{max} and $\varphi_{\mu max}$, when the chlorophyll concentration in the water varies from zone to zone, reduce the range of variation of their product, α'^{B}, which represents the initial slope.

For a variety of oceanic waters, the maximum chlorophyll-specific absorption coefficient (at about 440 nm, and expressed as m^2 (g Chl)$^{-1}$) varies as a function of the chlorophyll concentration, according to (Bricaud *et al.*, 1995)

$$a^*_{max} = 40.3(Chl)^{-0.33} \tag{1}$$

In their primary production model, and on the basis of their statistical studies, Wozniak *et al.* (1992) make $\varphi_{\mu max}$ vary with *Chl* according to

$$\varphi_{\mu max} = 0.05[(Chl)^{0.66}/(0.44 + (Chl)^{0.66})] \tag{2}$$

In this second relationship, *Chl* represents the surface layer concentration, considered as a bulk index of the trophic status. While both a^*_{max} and $\varphi_{\mu max}$ experience about a 10-fold change in opposite directions when Chl spans over 3 orders of magnitude (0.02–20 mg m^{-3}), their product remains confined within a much narrower interval (Fig. 15), and is centered around a typical value that actually is about half the α'^{B} value adopted in version 1 (Table 1). The reduced variability in this product is not really surprising to the extent that the increase in chlorophyll specific absorption, at low chlorophyll concentration, partly reflects the increase in non-photosynthetic pigments, which, in turn, leads to a reduction in quantum yield (according to its classic definition; see the Appendix). The above empirical equations, as well as the α'^{B} values derived from these equations, roughly account for the inter-site variations observed at sea (Table 2), but not for the depth-dependent intra-site variations

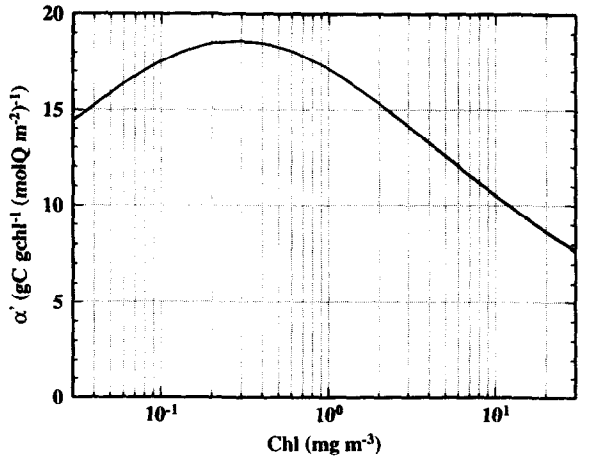

Fig. 15. As a function of the mean chlorophyll concentration (log scale), evolution of the maximal initial slope, α'^{B} (equation (A2b) in the Appendix), computed from equations (1) and (2) (see text).

(nor for the particular situation at the mesotrophic site during EUMELI no. 4). According to their authors, equations (1) and (2) are not intended to give fine details in a^*_{max} or $\varphi_{\mu max}$; considering the statistical uncertainties involved, the only aim is to quantify general trends for global applications.

The standard set of parameters could be modified according to the above results. In compatibility with Fig. 15, a unique mean α'^{B} value, for instance $16\,g\,C\,(g\,Chl)^{-1}$ (mol quanta $m^{-2})^{-1}$, could be simply adopted, valid for the 0.03–3 mg m^{-3} range, and more realistic than the previous one. Simultaneously the standard KPUR value could be increased up to 80 μmol quanta $m^{-2}\,s^{-1}$ to agree with the high near-surface values that were systematically observed at the three sites and also elsewhere for similar temperatures (Cullen *et al.*, 1992a). Such modifications, which lead to version 2 of the standard model, slightly change (actually diminish) the computed column integrated productions (Table 3), which become on average slightly smaller than those computed via version 1. For the 17 stations (cruises 3 and 4), the values computed via version 2 do not deviate (mean relative error $= -2\%$) from the measured ones; meanwhile the standard deviation ($\pm 18\%$) is notably reduced compared to that obtained with version 1.

With P^{B}_{max} slightly increased [4.6 instead of $3.4\,g\,C\,(g\,Chl)^{-1}\,h^{-1}$, at 20°C], the production within upper layers is accordingly enhanced, whereas smaller α'^{B} values entail a reduction of the production within the deep levels. As a consequence, the persistent failures in the representation of the vertical structures, previously noted when version 1 was used (e.g. Figs 6 and 8), are reduced greatly. The reconstructed vertical patterns appear close to those obtained with the actual parameters (Figs 10 and 11) and close to the measured values (Fig. 12). This improvement, not crucial when the column production is concerned, is valuable for other applications, for instance when studying the CO_2 partial pressure in the upper ocean, or the oxygen distribution and nutrient consumption. With respect to the numerical tests (displayed in Fig. 14 and Table 4), version 2 provides a much better agreement with the results and trends computed with the actual parameters (adjusted model) than those obtained using version 1.

The fact that a unique value of P^{B}_{max} is used for the entire column, if justified in well-mixed situations, becomes nonsense from the viewpoint of physiology in stratified

situations. It is nevertheless without numerical consequence as the light-saturated regime has little chance to be reached at depth. A relationship between P^B_{max} and the optical depth could be easily introduced in the computation scheme, in particular when stable stratification is expected. Such a relationship of ubiquitous validity, however, is not presently available for natural environments, although laboratory studies already provide some indications (see e.g. review in Geider, 1993). The KPUR–PAR relationship, as straightforwardly derivable from Fig. 8b, is an example of what would be needed everywhere. It is worth recalling that the problem of selecting appropriate P^B_{max} or KPUR values cannot be disconnected from that of the temperature effect on these parameters. It was always assumed here that the temperature effect is correctly accounted for by a unique Q_{10} value (but see Keller, 1989).

CONCLUSION

Some experimental deficiencies, in particular for the *in situ* determinations, prevent achievement of a better coincidence between measured and reconstructed primary productions using the measured photo-physiological parameters. The values in Table 4 can be interpreted in terms of error analysis or expected accuracy; they show that experimental uncertainties in P^B_{max} and α'^B, much below a factor of 2, (the technical reproducibility is better than 10%; see Babin *et al.*, 1994) affect the computed production in an insignificant way compared to the wider uncertainties attached to the *in situ* measurements (see e.g. Richardson, 1991). For instance, at a given site with similar day-to-day conditions (chlorophyll profile, irradiation), the outputs of the adjusted model were consistently similar and vertically smooth, while the reproducibility of the *in situ* ^{14}C measurements was often less convincing, with some unexplained features in the vertical profiles. Testing a computational method with regard to experimental "sea-truth" measurements, not exempted from their own weaknesses, is a recurrent problem.

Apart from the reservation about the relevance of the physiological parameters used as inputs (because of the difference in physiological reponses involved in short or long incubations), there is no reason to challenge the capacity of an adjusted model when physics and P versus E curves are well represented in the model. This confidence in the capacity of such a model, when applied to specific cases, does not solve the problem of generalized application, particularly in conjunction with global satellite information. The need for generic model(s), based on standard photo-physiological parameters, either constant or simply predictable in their variations, still exists and was a motivation of the present work.

As a result of sensitivity analyses covering diverse trophic regimes, also by accounting for recent empirical relationships established for the world ocean, a modified set of photo-physiological parameters is proposed. It is implemented in the previous model (Morel, 1991) which is left unchanged in its structure. With these modifications, restricted to the numerical values of KPUR (at 20°C) and α'^B, this model is referred to as version 2. In this version, the model aims at relating the photo-physiological parameters to remote observables; indeed, scaling α'^B and $\varphi_{\mu max}$ with the chlorophyll concentration (detectable from space), and varying P^B_{max} with temperature (also detectable), are attempts towards such a goal. When this version was operated, a better reconstruction of the primary production profile was obtained and the retrieval of the values was close to that offered by the adjusted model in very contrasted situations. Moreover, in terms of integrated production, this set of parameters has led to the best agreement with measured values and the smallest standard

deviation (Table 3). The improved capacity of this version, still to be confirmed, provides an increased confidence in the capacity of predicting the column integrated carbon fixation, as well as of simulating more accurately the depth-dependent exchange between the inorganic and organic carbon pools.

Acknowledgements—This work, which is a contribution to the EUMELI program, received financial support from the Agencies funding the JGOFS–France activities, and from CNRS–INSU in particular. The crew of R.V. *l'Atalante* is warmly thanked. We wish to thank M. R. Lewis and an anonymous reviewer who helped, by their very constructive comments, in shaping this work, A. Bricaud for her advice in the progress of this work, and J. Dolan for improving the English in the final version.

REFERENCES

Antoine D. and A. Morel (1996) Oceanic primary production: 1. Adaptation of a spectral light–photosynthesis model in view of application to satellite chlorophyll observations. *Global Biogeochemical Cycles*, **10**, 42–55.

Antoine D., A. Morel and J. M. André (1995) Algal pigment distribution and primary production in the eastern Mediterranean as derived from Coastal Zone Color Scanner observations. *Journal of Geophysical Research*, **100**, 16,193–16,209.

Antoine D., J. M. André and A. Morel (1996) Oceanic primary production: 2. Estimation at global scale from satellite (Coastal Zone Color Scanner) chlorophyll. *Global Biogeochemical Cycles*, **10**, 56–69.

Babin M., A. Morel and A. Gagnon (1994) An incubator designed for extensive and sensitive measurements of phytoplankton photosynthetic parameters. *Limnology and Oceanography*, **39**, 496–510.

Babin M., A. Morel, H. Claustre, A. Bricaud, Z. Kolber and P. G. Falkowski (1996) Nitrogen- and irradiance-dependent variations of the maximum quantum yield of carbon fixation in eutrophic, mesotrophic and oligotrophic marine systems. *Deep-Sea Research I*, **43**, 1241–1272.

Bannister T. T. and A. D. Weidemann (1984) The maximum quantum yield of phytoplankton photosynthesis *in situ*. *Journal of Plankton Research*, **6**, 275–294.

Berthon J. F. and A. Morel (1992) Validation of a spectral light-photosynthesis model and use of the model in conjunction with remotely sensed pigment observations. *Limnology and Oceanography*, **37**, 781–796.

Bienfang P., J. P. Szyper, M. Y. Okamo and E. K. Noda (1984) Temporal and spatial variability of phytoplankton in a subtropical system. *Limnology and Oceanography*, **29**, 527–539.

Bricaud A. and D. Stramski (1990) Spectral absorption coefficients of living phytoplankton and nonalgal biogenous matter: A comparison between the Peru upwelling area and Sargasso Sea. *Limnology and Oceanography*, **35**, 562–582.

Bricaud A., A. Morel and J. M. André (1987) Spatial/temporal variability of algal biomass and potential productivity in the Mauritanian upwelling zone, as estimated from CZCS data. *Advances in Space Research*, **7**, 53–62.

Bricaud A., M. Babin, A. Morel and H. Claustre (1995) Variability in the chlorophyll-specific absorption coefficients of natural phytoplankton: Analysis and parameterization. *Journal of Geophysical Research*, **100**(C7), 13,321–13,332.

Butler L. W. (1962) Absorption of light by turbid materials. *Journal of the Optical Society of America*, **52**, 292–299.

Carder K. L., S. K. Hawes, K. A. Baker, R. C. Smith, R. G. Steward and B. G. Mitchell (1991) Reflectance model for quantifying chlorophyll *a* in the presence of productivity degradation products. *Journal of Geophysical Research*, **96**, 20,599–20,611.

Claustre H. (1994) The trophic states of various oceanic provinces as revealed by phytoplankton pigment signatures. *Limnology and Oceanography*, **39**, 1207–1211.

Claustre H. and J. C. Marty (1995) Specific phytoplankton biomasses and their relation to primary production in the tropical North Atlantic. *Deep-Sea Research I*, **42**, 1475–1493.

Cleveland J. S. (1995) Regional models for phytoplankton absorption as a function of chlorophyll *a* concentration. *Journal of Geophysical Research*, **100**, 13,333–13,344.

Côte B. and T. Platt (1984) Utility of the light–saturation curve in an operational model for quantifying the effects of environmental conditions on phytoplankton photosynthesis. *Marine Ecology Progress Series*, **18**, 57–66.

Cullen J. J. and M. R. Lewis (1988) The kinetics of algal photoadaptation in the context of vertical mixing. *Journal of Plankton Research*, **10**, 1039–1063.

Cullen J. J., M. R. Lewis, C. O. Davis and R. T. Barber (1992a) Photosynthetic characteristics and estimated growth rates indicate grazing is the proximate control of primary production in the Equatorial Pacific. *Journal of Geophysical Research*, **97**, 639–654.

Cullen J., X. Yang and H. L. Macintyre (1992b) Nutrient limitation and marine photosynthesis. In: *Primary productivity and biogeochemical cycles in the sea*, P. G. Falkowski and A. D. Woodhead, editors, Plenum Press, New York, pp. 69–88.

Dandonneau Y. and A. Le Bouteiller (1992) A simple and rapid device for measuring planktonic primary production by *in situ* sampling, and ^{14}C injection and incubation. *Deep-Sea Research*, **39**, 795–803.

Eppley R. W. (1972) Temperature and phytoplankton growth in the sea. *Fisheries Bulletin*, **70**, 1063–1084.

Falkowski P. G., D. Ziemann, Z. Kolber and P. K. Bienfang (1991) Role of eddy pumping in enhancing primary production in the ocean. *Nature*, **352**, 55–58.

Fee E. J. (1973) A numerical model for determining integral primary production and its application to Lake Michigan. *Journal of Fisheries Research Board of Canada*, **30**, 1447–1468.

Feldman G. C., N. Kuring, C. Ng, W. Esaias, C. McClain, J. Elrod, N. Maynard, D. Endres, R. Evans, J. Brown, S. Walsh, M. Carle and G. Podesta (1989) Ocean color: availability of the global data set. *EOS*, **70**, 634.

Geider R. J. (1993) Quantitative phytoplankton physiology: implications for primary production and phytoplankton growth. *ICES Marine Sciences Symposium*, **197**, 52–62.

Geider R. J., R. M. Greene, Z. Kolber, H. L. Mcintyre and P. G. Falkowski (1993) Fluorescence assessment of the maximum quantum efficiency of photosynthesis in the western North Atlantic. *Deep-Sea Research I*, **40**, 1205–1224.

Gordon H. R. and A. Morel (1983) *Remote assessment of ocean color for interpretation of satellite visible imagery: a review*. Springer-Verlag, New York.

Harrison W. G., T. Platt and M. R. Lewis (1985) The utility of light–saturation models for estimating marine primary productivity in the field: a comparison with conventional "simulated" *in situ* methods. *Canadian Journal of Fisheries and Aquatic Sciences*, **42**, 864–872.

Henley W. J. (1993) Measurements and interpretation of photosynthesis light–response curves in algae in the context of photoinhibition and diel changes. *Journal of Phycology*, **29**, 729–739.

Jassby A. D. and T. Platt (1976) Mathematical formulation of the relationship between photosynthesis and light for phytoplankton. *Limnology and Oceanography*, **21**, 540–547.

JGOFS/SCOR (1990) Science Plan, Joint Global Ocean Flux Studies. JGOFS Report Series 5, SCOR editor, The Johns Hopkin's University, Baltimore.

Jitts H. R., A. Morel and Y. Saijo (1976) The relation of oceanic primary production to available photosynthetic irradiance. *Australian Journal of Marine Freshwater Research*, **27**, 441–454.

Keller A. A. (1989) Modeling the effects of temperature, light, and nutrients on primary productivity: an empirical and a mechanistic approach compared. *Limnology and Oceanography*, **34**, 82–95.

Kishino M., M. Takahashi, N. Okami and S. Ichimura (1985) Estimation of the spectral absorption coefficients of phytoplankton in the sea. *Bulletin of Marine Science*, **37**, 634–642.

Kishino M., N. Okami, M. Takahashi and S. Ichimura (1986) Light utilization efficiency and quantum yield of phytoplankton in a thermally stratified sea. *Limnology and Oceanography*, **31**, 557–566.

Lande R. and M. R. Lewis (1989) Models of photoadaptation and photosynthesis by algal cells in a turbulent mixed layer. *Deep-Sea Research*, **36**, 1161–1175.

Lewis M. R. (1992) Satellite ocean color observations of global biogeochemical cycles. In: *Primary productivity and biogeochemical cycles in the sea*, P. G. Falkowski and A. D. Woodhead, editors, Plenum Press, New York, pp. 139–153.

Lewis M. R., E. P. Horne, J. J. Cullen, N. S. Oakey and T. Platt (1984) Turbulent motion may control phytoplankton photosynthesis in the upper ocean. *Nature*, **311**, 49–50.

Lewis M. R., R. E. Warnock and T. Platt (1985) Absorption and photosynthetic action spectra for natural phytoplanktonic population: implication for production in the open ocean. *Limnology and Oceanography*, **30**, 794–806.

Lewis M. R., O. Ulloa and T. Platt (1988) Photosynthetic action, absorption and quantum yield spectra for a natural population of Oscillatoria in the North Atlantic. *Limnology and Oceanography*, **33**, 92–98.

Longhurst A., S. Sathyendranath, T. Platt and C. Caverhill (1995) An estimate of global primary production in the ocean from satellite radiometer data. *Journal of Plankton Research*, **17**, 1245–1271.

Morel A. (1982) Optical properties and radiant energy in the waters of the Guinea dome and the Mauritanian

upwelling area in relation to primary production. *Rapports et Procés-Verbaux des Réunions du Conseil Permanent pour l'Exploration de la Mer*, **180**, 94–107.

Morel A. (1988) Optical modeling of the upper ocean in relation to its biogenous matter content (case 1 waters). *Journal of Geophysical Research*, **93**, 10,749–10,768.

Morel A. (1991) Light and marine photosynthesis: a spectral model with geochemical and climatological implications. *Progress in Oceanography*, **26**, 263–306.

Morel A. and J. M. André (1991) Pigment distribution and primary production in the Western Mediterranean as derived and modeled from Coastal Zone Color Scanner observations. *Journal of Geophysical Research*, **96**, 12,685–12,698.

Morel A. and J. F. Berthon (1989) Surface pigments, algal biomass profiles and potential production of the euphotic layer: relationships reinvestigated in view of remote-sensing applications. *Limnology and Oceanography*, **34**, 1545–1562.

Partensky F., J. Blanchot, F. Lantoine, J. Neveux and D. Marie (1996) Vertical structure of picophytoplankton at different trophic sites of the tropical northeastern Atlantic Ocean. *Deep-Sea Research I*, **43**, 1191–1213.

Platt T. C. and S. Sathyendranath (1988) Oceanic primary production, estimation by remote sensing at local and regional scales. *Science*, **241**, 1613–1620.

Platt T., S. Sathyendranath, C. M. Caverhill and M. R. Lewis (1988) Ocean primary production and available light: further algorithms for remote sensing. *Deep-Sea Research*, **35**, 855–879.

Platt T., C. Caverhill and S. Sathyendranath (1991) Basin-scale estimates of oceanic primary production by remote sensing: the north Atlantic. *Journal of Geophysical Research*, **96**, 15,147–15,159.

Raimbault P., G. Slawyk, B. Coste and J. Fry (1990) Feasibility of using an automatic procedure for the determination of seawater nitrate in the 0–100 nM range: examples from field and culture. *Marine Biology*, **104**, 347–351.

Richardson K. (1991) Comparison of ^{14}C primary production determinations made by different laboratories. *Marine Ecology Progress Series*, **72**, 189–201.

Sathyendranath S., T. Platt, C. M. Caverhill, R. E. Warnock and M. R. Lewis (1989) Remote sensing of oceanic primary production: computations using a spectral model. *Deep-Sea Research*, **36**, 431–453.

Sathyendranath S., A. Longhurst, C. M. Caverhill and T. Platt (1995) Regionally and seasonally differenciated primary production in the North Atlantic. *Deep-Sea Research I*, **42**, 1773–1802.

Smith R. C., B. B. Prézelin, R. R. Bidigare, M. R. Lewis and K. S. Baker (1989) Bio-optical modelling of photosynthetic production. *Limnology and Oceanography*, **34**, 1526–1546.

Sosik H. M. and B. G. Mitchell (1995) Light absorption by phytoplankton, photosynthetic pigments and detritus in the California current system. *Deep-Sea Research I*, **42**, 1717–1748.

Speth P. and H. Detlefsen (1982) Meteorological influences on upwelling off northwest Africa. *Rapport et Procès-Verbaux des Réunions du Conseil International pour l'Exploration de la Mer*, **180**, 29–34.

Talling J. F. (1957) The phytoplankton population as a compound photosynthetic system. *New Phytologist*, **56**, 133–149.

Wozniak B. and M. Ostrowska (1990) Optical absorption properties of phytoplankton in various seas. *Oceanologia*, **29**, 117–146.

Wozniak B., J. Dera and O. Koblentz-Mischke (1992) Modeling the relationship between primary production, optical properties and nutrients in the sea (as a basis for indirectly estimating primary production). *Ocean Optics 11, Proceeding of SPIE — The International Society for Optical Engineering*, **1750**, 246–275.

APPENDIX

Relationships between the physiological parameters derived from the P–E *curve and those used in the primary production model*

An idealized P–E curve is shown in Fig. 16(a), where the carbon fixation rate is normalized with respect to the biomass, P^B (usually the chlorophyll mass is used when normalizing), and where the irradiance E is expressed as Photosynthetically Available Radiation, PAR. P^B_{max} is the maximum rate and E_K (Talling, 1957) is a parameter (dimension of irradiance) which is used to characterize the onset of the light-saturated regime. The initial slope of the curve, within the light-limited regime, is generally denoted α^B (superscript B for biomass normalization). There exist the following relationships

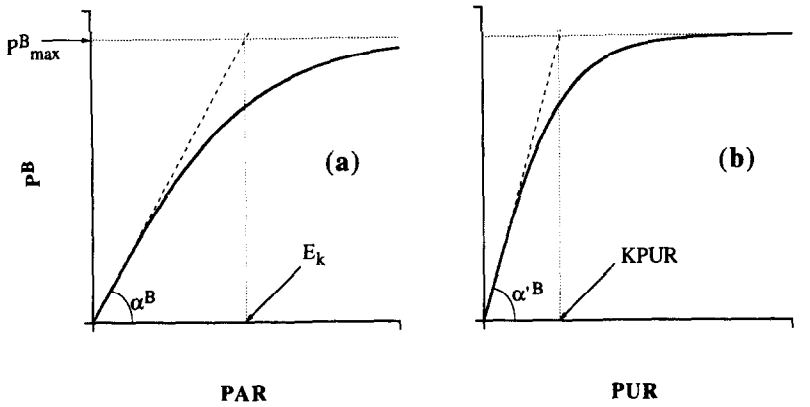

Fig. 16. Idealized curve of photosynthetic rate as a function of photosynthetically available radiation (PAR) or usable radiation (PUR), and relevant quantities with their symbols.

(dimension of irradiance) which is used to characterize the onset of the light-saturated regime. The initial slope of the curve, within the light-limited regime, is generally denoted α^B (superscript B for biomass normalization). There exist the following relationships

$$P^B_{max}/E_k = \alpha^B \tag{A1a}$$

$$\alpha^B = 12\bar{a}^*\varphi_{\mu max} \tag{A2a}$$

The first one is purely geometrical, whereas the second one states that at vanishing irradiance P^B is proportional to the incident energy through both an absorption coefficient and a yield. The latter is generally expressed as mol C (mol quanta)$^{-1}$, so that the factor 12 (g C mol^{-1}) is needed if the carbon fixation is expressed as a mass fixation. The mean absorption coefficient, a, is normalized with respect to Chl (star) and in relevance (overbar) to the spectral composition of the available radiation, PAR (λ); it is defined as

$$\bar{a}^* = \int_{\lambda_1}^{\lambda_2} a^*(\lambda)\mathrm{PAR}(\lambda)\mathrm{d}\lambda / \int_{\lambda_1}^{\lambda_2} \mathrm{PAR}(\lambda)\mathrm{d}\lambda \tag{A3}$$

The limits of the integrals are in general 400 and 700 nm, and the integral in the denominator provides PAR; $a^*(\lambda)$ represents the spectrally varying chlorophyll-specific absorption coefficient of algae, and thus $\bar{a}$ is a spectrally averaged algal coefficient. This averaged coefficient obviously varies with the shape of the PAR (λ) spectrum used as a weighting function, and so do α^B and therefore E_K, since P^B_{max} is unaffected by the spectral composition of radiant energy. The straightforward consequence of such dependencies is that any interpretation or comparison of α^B and E_K values found in the literature, and determined in various experimental conditions, are impossible, as far as PAR (λ) is not known or specified, and if PAR (λ) is known, as far as $a^*(\lambda)$ has not been determined. This difficulty is often ignored.

A way to circumvent this drawback is to use the Photosynthetic Usable Radiation, PUR, instead of PAR (Fig. 16(b)). PUR represents the fraction of PAR that can be absorbed by algae and is computed as

$$\mathrm{PUR} = \int_{400}^{700} \mathrm{PAR}(\lambda)\, A^*(\lambda)\mathrm{d}\lambda \tag{A4}$$

The weighting function $A^*(\lambda)$, defined in the interval [0; 1], is the ratio

$$A^*(\lambda) = a^*(\lambda)/a^*_{max} \tag{A5}$$

where a^*_{max} is the maximal value of the $a^*(\lambda)$ spectrum. Rearranging equations (A3), (A4) and (A5), it follows that

$$\bar{a}^*\mathrm{PAR} = a^*_{max}\mathrm{PUR} \tag{A6}$$

In reference to Fig. 16(b), where P^B is plotted as a function of PUR, the quantities similar to those in equations (A1) and (A2) are now the primed quantities as follows

$$P^{B}_{max}/E'_{K} = \alpha'^{B} \tag{A1b}$$

and

$$\alpha'^{B} = 12\varphi_{\mu max}a^{*}_{max} \tag{A2b}$$

In contrast to α^{B}, the slope α'^{B} is unique and independent of the spectral quality of the incident radiation, and both are related through

$$\alpha^{B}/\alpha'^{B} = \bar{a}^{*}/a^{*}_{max} \tag{A7}$$

The primary production model (Morel, 1991) makes use of a dimensionless irradiance, x, defined as the ratio of PUR to a certain normalizing value denoted KPUR; the P versus E curve is then described via a function $f(x)$, defined within interval [1; 0], which expresses the variations of the realized quantum yield at any point of the curve and reaches its maximal value (unity) at vanishing irradiance, when x tends toward 0. According to equation (22b) in the above reference, the maximum rate of carbon fixation is expressed as

$$P^{B}_{max} = 12a^{*}_{max}\varphi_{\mu max}[x.f(x)]_{max}\mathrm{KPUR} = \alpha'^{B}[x.f(x)]_{max}\mathrm{KPUR} \tag{A8}$$

so that KPUR = E'_{K}, to the extent that the maximal value attained by the product within the bracket could be strictly equal to 1. It is the case when the dimensionless function $f(x)$ is derived from any mathematical representation of the P–E curve that does not include photoinhibition. From equations (A1a) and (A1b) it results:

$$\alpha'^{B}E'_{K} = \alpha^{B}E_{K}$$

therefore KPUR ($= E'_{K}$) can be expressed as a function of E_{K} by using equation (A7)

$$\mathrm{KPUR} = E_{K}\frac{\bar{a}^{*}}{a^{*}_{max}} \tag{A9}$$

From the experimental values of E_{K}, and $\bar{a}^{*}$ and a^{*}_{max}, KPUR can be computed before being entered into the model. Note that the above $\bar{a}^{*}/a^{*}_{max}$ ratio was about 0.36, 0.44 and 0.33 at the eutrophic, mesotrophic and oligotrophic sites, respectively.The $f(x)$ function used here is derived from the Jassby and Platt (1976) formulation, based on a hyperbolic tangent function. The shape of the resulting P–E curve is very close (with, however, an enhanced convexity) to that resulting from the Webb *et al.* exponential formulation (previously used and cited in Morel, 1991). Both formulations actually have been used in parallel in the model with minute differences in terms of integrated primary production (a few per cent and at the most + 8%, in favor of the hyperbolic tangent function). In the P versus E determinations discussed and used in the present study, photoinhibition was not detected. The *in situ* determinations did not suggest the occurrence of such an effect. As shown elsewhere (Antoine and Morel, 1996), inclusion or exclusion of this effect has only a minor impact on the computed integrated production, well below the uncertainties following from the choice of more crucial parameters (such as α'^{B} and KPUR). In the same reference, it is also shown that changing the shape of the chlorophyll-specific absorption spectrum of algae (the $A^{*}(\lambda)$ function above), even when extrema are considered (pure diatoms and pure prochlorophyte populations), has a negligible influence upon the computed production. Therefore the actual shapes, which actually differ at the three sites (see Babin *et al.*, 1996), have been replaced by the single standard $A^{*}(\lambda)$ shape adopted by Morel (1991), with an accepted error of a few per cent. It must be added that if (in equation (A2a)) the quantum yield is based on the classic definition, i.e. in reference to all photons absorbed, including those absorbed by pigments not active in photosynthesis, $\varphi_{\mu max}$ is varying (Sosik and Mitchell, 1995). It is depressed by the presence of non-photosynthetic pigments (such as photoprotective ones), even if the photosynthetic reaction centers are still processing the absorbed energy by the photosynthetic pigments with the maximum yield. This remark also entails that $\varphi_{\mu max}$ is not spectrally constant, although it is considered, in practice, as non-spectral in the present model.